Research Paper

THEMED ISSUE: Mantle to Surface Dynamics during the Transition from Subduction to Collision to Tectonic Escape: Results from the Continental Dynamics-Central Anatolian Tectonics (CD-CAT) Project

GEOSPHERE

GEOSPHERE, v. 17, no. 6

https://doi.org/10.1130/GES02329.1

8 figures; 2 tables; 1 set of supplemental files

CORRESPONDENCE: furman@psu.edu

CITATION: Furman, T., Hanan, B.B., Sjoblom, M.P., Kürkcüoğlu, B., Sayit, K., Şen, E., Alıcı Şen, P., and Yürür, T., 2021, Evolution of mafic lavas in Central Anatolia: Mantle source domains: Geosphere, v. 17, no. 6, p. 1631–1646, https://doi.org/10.1130/GES02329.1.

Science Editor: Shanaka de Silva
Associate Editor: G. Lang Farmer

Received 10 August 2020
Revision received 10 May 2021
Accepted 18 June 2021

Published online 4 November 2021

Evolution of mafic lavas in Central Anatolia: Mantle source domains

Tanya Furman[1], Barry B. Hanan[2], Megan Pickard Sjoblom[1,3], Biltan Kürkcüoğlu[4], Kaan Sayit[5], Erdal Şen[4], Pinar Alıcı Şen[6], and Tekin Yürür[4]

[1]Department of Geosciences, Pennsylvania State University, University Park, Pennsylvania 16802, USA
[2]Department of Geological Sciences, San Diego State University, San Diego, California 92182, USA
[3]Department of Geology, Brigham Young University–Idaho, Rexburg, Idaho 83460, USA
[4]Department of Geological Engineering, Hacettepe University, 06800 Beytepe–Ankara, Turkey
[5]Department of Geological Engineering, Middle East Technical University, 06800 Çankaya–Ankara, Turkey
[6]General Directorate of Mineral Research and Exploration, 06800 Balgat–Ankara, Turkey

ABSTRACT

We present new Sr-Nd-Pb-Hf isotopic data on mafic lavas from the Sivas, Develidağ, Erciyes, and Erkilet volcanic complexes in central Turkey and Tendürek in eastern Turkey to evaluate the mantle sources for volcanism in the context of the geodynamic evolution of the Anatolian microplate. Early Miocene through Quaternary volcanism in Western Anatolia and latest Miocene through Quaternary activity in Central Anatolia were dominated by contributions from two distinct source regions: heterogeneous metasomatized or subduction-modified lithosphere, and roughly homogeneous sublithospheric ambient upper mantle; we model the source contributions through mixing between three end members. The sublithospheric mantle source plots close to the Northern Hemisphere reference line (NHRL) with radiogenic $^{206}Pb/^{204}Pb$ of ~19.15, while the other contributions plot substantially above the NHRL in Pb isotope space. The lithospheric source is heterogeneous, resulting from variable pollution by subduction-related processes likely including direct incorporation of sediment and/or mélange; its range in radiogenic isotopes is defined by regional oceanic sediment and ultrapotassic melts of the subcontinental lithospheric mantle. The geochemical impact of this contribution is disproportionately large, given that subduction-modified lithosphere and/or ocean sediment dominates the Pb isotope signatures of mafic Anatolian lavas. Subduction of the Aegean or Tethyan seafloor, associated with marked crustal shortening, took place throughout the region until ca. 16–17 Ma, after which time broad delamination of the thickened lower crust and/or the Tethyan slab beneath Central Anatolia allowed for sediment and/or mélange and slab-derived fluids to be released into the overlying evolving modified mantle. Aggregation of melts derived from both mantle and lithospheric domains was made possible by upwelling of warm asthenospheric material moving around and through the complexly torn younger Aegean-Cyprean slab that dips steeply to the north beneath southern Anatolia.

Tanya Furman https://orcid.org/0000-0002-2134-3438
Biltan Kürkcüoğlu https://orcid.org/0000-0001-8927-4486
Erdal Şen https://orcid.org/0000-0002-9172-9926
Pinar Alıcı Şen https://orcid.org/0000-0002-2457-7280
Tekin Yürür https://orcid.org/0000-0002-3077-8249

INTRODUCTION

Continental assembly and breakup are key components of crustal evolution, and their effects are seen in the rocks of orogenic belts across the globe. The Alpine-Himalayan orogen is one such region, in which complex convergence of continental masses has been accompanied by the growth of major mountain belts and followed locally by periods of extensional collapse. Central and Western Anatolia are regions of post-collisional volcanism within this major orogen where both calc-alkaline and alkaline mafic lavas have erupted episodically from the early Miocene to the present. The transition from convergence to extension, and the complex evolution of the continental lithosphere and sublithosphere that accompanied this change, are manifest in the geochemical and isotopic signatures of Anatolian mafic lavas that are the focus of this work.

The thermal effects of rifting or post-orogenic crustal relaxation can initiate melting of hydrated lithosphere that was metasomatized during previous subduction events, given that metasomatic fluids in suprasubduction zones can produce abundant veins rich in fluid-mobile trace elements within the lithospheric mantle. In subduction zones, both slab-derived fluids and sediment-mélange packages may mix with mantle wedge material and contribute to the overall chemistry of continental volcanics (e.g., Behn et al., 2011; Nielsen and Marschall, 2017). At a larger scale, lithospheric thickening can occur in any magmatic environment through the underplating of cumulates, and in subduction settings through the accretion of slabs to the underside of an existing crustal section. Given the propensity of continental material to rift along pre-existing zones of convergent and transverse movement, intraplate extensional mafic lavas likely interact with lithospheric materials that record earlier subduction processes and thus the geochemical consequences of continental evolution.

Recent geophysical studies have resolved a complex network of subducted materials beneath Anatolia. Tomographic images reveal fast seismic anomalies beneath Anatolia that correspond to the subducted portion of the African lithosphere along the Cyprean and Aegean trenches (Biryol et al., 2011; Bartol and Govers, 2014; Govers and Fichtner, 2016). The two slabs are clearly separated south of Anatolia; both dip to the north, and they merge at depth beneath mid-latitude Anatolia. It is significant that tomograms from depths

below 500 km show that the separate fast anomalies (Cyprean and Aegean slabs) merge to form a continuous belt that extends beneath all of Central Anatolia and flattens out along the mantle transition zone (~660 km depth). The implication is that this feature is a single slab that sank beneath the present-day İzmir-Ankara-Erzincan suture, and Bartol and Govers (2014) suggested it represents delaminated lithospheric mantle (i.e., the northern Neotethys slab) that sank into the deeper mantle in the early Miocene (ca. 20–15 Ma). Delamination of this slab was followed by slab rollback to the present location south of Cyprus, while in Western Anatolia, it has resulted in extension both on land and in the eastern Aegean Sea. Slabs beneath both Central and Western Anatolia show geophysical evidence of tearing that allows warm asthenosphere to penetrate to shallow levels both through and around the subducted materials.

In this study, we report new major and trace element abundances and Sr-Nd-Pb-Hf isotopic data for late Miocene to recent mafic volcanic rocks from Central Anatolia and interpret them within the geodynamic context of complex slab configurations beneath the region; our new data are considered in the context of published data for Miocene and younger lavas from both Central and Western Anatolia (Alıcı et al., 1998, 2002; Kürkçüoğlu et al., 1998, 2001; Parlak et al., 2001; Şen et al., 2004; Chakrabarti et al., 2012; Aldanmaz et al., 2015; Reid et al., 2017; Di Giuseppe et al., 2018; Kocaarslan and Ersoy, 2018). Our goal is to provide a better understanding of the mantle source domains that contribute to volcanism in these areas, and specifically to explore relationships between major lithospheric and sublithospheric features as they relate to the tectonic evolution of Anatolia. Recent isotopic studies of Anatolian mafic lavas have attributed their genesis to contributions from depleted mid-ocean-ridge (MORB)–like mantle and a subduction modified oceanic island basalt (OIB)–like source domain containing fluids or melts associated with subducted sediments (e.g., Chakrabarti et al., 2012; Reid et al., 2017). Here, we extend the geographic and temporal scope of mafic lavas under consideration, allowing us to document source evolution and distribution in a complex tectonic environment affected by regional-scale lithospheric delamination subsequent to the closure of Neotethys and the onset of southwestward movement of the Anatolian microplate (Bartol and Govers, 2014; Göğüs et al., 2017). Ultimately, the insights provided through the geochemical characteristics of Anatolian mafic volcanism allow us to unravel the geochemical and tectonic development of dynamic orogenic and post-orogenic regions.

TECTONIC AND VOLCANIC HISTORY

Anatolia is part of the Alpine-Himalayan orogenic belt, formed by tectonic juxtaposition of pieces of continental lithosphere during the Cenozoic closure and terminal suturing of the northern and southern branches of the Neotethys Ocean. Between the Cretaceous and late Eocene (ca. 100–34 Ma), the majority of the convergence between Africa and Arabia-Eurasia was accommodated by northward subduction of the northern Neotethys Ocean along the İzmir-Ankara-Erzincan suture zone (IAESZ; Fig. 1; Şengör and Yılmaz, 1981; Okay and Tüysüz, 1999; Bartol and Govers, 2014). By the late Paleocene, the northern portion of the ocean was closed along this suture, allowing for the terminal collision of the Eurasian plate with the Anatolian-Iranian Platform, which had approached from the south. The North Anatolian fault zone follows this northern Neotethyan suture, while more complex subduction of the southern Neotethys is manifest in the Aegean and Cyprean trenches immediately south of Anatolia.

Subduction of the African plate and closure of the southern Neotethys began south of Cyprus by the early Miocene, continuing through the mid-Miocene in the east and the early Quaternary in the west (Dewey et al., 1989). Final collision along the Bitlis-Zagros suture zone (Fig. 1) halted northward movement of the Arabian plate with respect to Africa and thickened the crust across the Anatolian-Iranian Platform by as much as 2 km (e.g., Yılmaz et al., 1993). Northward subduction of African lithosphere occurs at present along the Aegean and Cyprean trenches, which are separated by the Isparta Angle in southern Anatolia. Subduction along the Cyprus section of the trench is influenced by the collision of the Eratosthenes Seamount, which obstructs descent of the African plate, leading to steep subduction and tearing of the downgoing slab (Wortel and Spakman, 1992).

The interplay between northern Neotethyan slab delamination and southern Neotethyan subduction sets the stage for modern volcanism across Anatolia. Subsequent to the regional-scale delamination event, an influx of asthenosphere into the uppermost mantle resulted in broad heating and uplift of the Anatolian plateau, manifest today in an anomalously thin lithospheric mantle (30–40 km; Govers and Fichtner, 2016) and high heat flow (e.g., Keskin, 2003). Although delamination may have occurred at different times across Anatolia, there is no compelling evidence to support an age progression (Bartol and Govers, 2014). In Western Anatolia, post–mid-Miocene extension and volcanism have been broadly associated with slab rollback along the Hellenic Trench since ca. 12 Ma (Meulenkamp et al., 1988) and lithospheric delamination (Biryol et al., 2011; Bartol and Govers, 2014). Slab rollback across the Aegean extensional province reflects the differential convergence rates between Africa and Europe (~10 mm/yr) and along the Hellenic Trench (~40 mm/yr; McClusky et al., 2000). Thus, early Miocene mafic volcanism in Western Anatolia followed almost immediately upon the heels of delamination, while the neotectonic environment of Western Anatolia is dominated by extension related to rollback of the Hellenic-Aegean slab.

Mio-Pliocene through recent faulting and volcanism in Central Anatolia are consequences of internal extension governed primarily by "escape tectonics" as the microplate moves westward at a rate of ~15 mm/yr along major strike-slip fault systems (Reilinger et al., 1997) with ascent of mafic melts along crustal faults (e.g., Notsu et al., 1995). The most recent phase of volcanism in Central Anatolia ensued several million years following regional slab delamination, presumably related to slow heating of the lower lithosphere, and post-dates two pulses of ignimbrite activity dated at 9–8 Ma and 7–5 Ma in the Cappadocian volcanic province (Innocenti et al., 1975; Temel et al., 1998; Aydar et

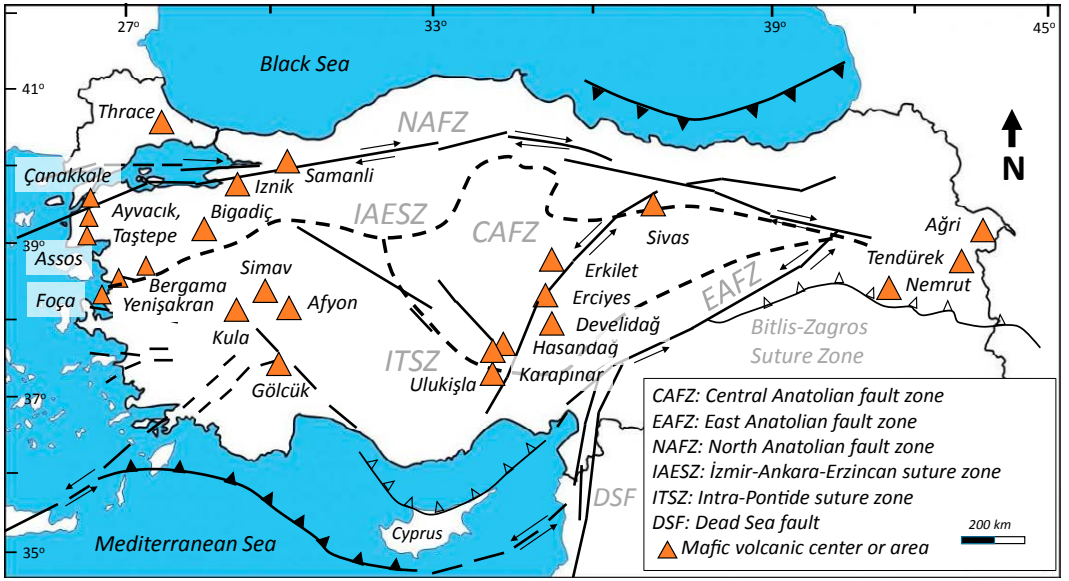

Figure 1. Neotectonic map of Anatolia and surrounding region including major fault systems and volcanic areas (after Çoban, 2007). Arrows indicate relative plate motions. Triangles show selected Miocene–Quaternary volcanoes and the Cretaceous Ulukişla volcanic area.

al., 2012). This phase of activity began with growth of multi-stage Miocene through Quaternary calc-alkaline andesitic stratovolcanoes associated with transtensional pull-apart basins including Erciyes and Hasandağ (Kürkçüoğlu et al., 1998; Şen et al., 2004; Fig. 1) and continued through the Quaternary at scattered mafic and felsic vents with an increasing representation of alkali olivine basalts (e.g., adjacent to Hasandağ and Karapınar, 0.6–0.2 Ma; Reid et al., 2017).

We present new geochemical and isotopic analyses of the mafic volcanic rocks from several volcanic areas including Sivas, the northernmost magmatic province in Central Anatolia (Fig. 1). Parlak et al. (2001) referred to Sivas volcanism overall as Plio-Pleistocene and the basalts as Plio-Quaternary, but K-Ar ages of 3.3 Ma (Türkecan et al., 2000) and 4.0 ± 1.2 to 5.88 ± 0.77 Ma (Platzman et al., 1998) suggest volcanism developed in latest Miocene to early Pliocene time. Sivas lacks a stratovolcanic edifice but rather comprises numerous small-volume mildly alkaline mafic flows (Parlak et al., 2001; Kocaarslan and Ersoy, 2018). Primitive basanites appear to be restricted to the northwestern portion of the study area, while basaltic through trachyandesitic lavas are common in the southeast; the two eruptive groups are separated by the Kızılırmak River, which overlies a major strike-slip fault associated with the IAESZ (Kürkçüoğlu et al., 2015). Compositional differences among Sivas lavas are variously attributed to crustal contamination (Parlak et al., 2001; Kocaarslan and Ersoy, 2018) or distinct thermal and magmatic environments across the suture (Kürkçüoğlu et al., 2015).

Our data set also includes two new basalts from the youngest Plio-Quaternary phase of activity at Erciyes stratovolcano (Notsu et al., 1995) and undated mafic lavas from Erkilet and Develidağ (Fig. 1). The Erkilet and Develidağ volcanic complexes are commonly referred to as Mio-Pliocene in age (e.g., LePennec et al., 1994), although no comprehensive age determinations have been published. Dönmez et al. (2003) reported a K-Ar age of 5.3 Ma on a Develidağ andesite, and Türkecan et al. (1998) reported a K-Ar age of 3.1 Ma on an Erkilet lava but provided no compositional or stratigraphic metadata.

In this paper, we use the Sr-Nd-Pb-Hf radiogenic isotope compositions of early Miocene through Quaternary mafic lavas from Central and Western Anatolia to determine the origin and geodynamic evolution of their mantle sources and to relate their occurrence to the regional tectonic history of continental assembly and post-orogenic extension. These results enable us to compare mantle source evolution across Anatolia, and in particular, to explore the contribution from subducted sediments and to identify the geochemical and isotopic end members involved.

METHODS

Samples of visibly fresh lavas were cut into slabs with any weathered portions removed and reduced to ~5–7 mm pieces using an alumina ceramic mini-crusher. Powders were prepared by grinding in a tungsten carbide disc mill for 30–90 s. Whole-rock analyses for major and minor elements (including Ba and Sr) were obtained by direct current plasma spectrometry on an ARL-Fisons Spectraspan 7; remaining trace elements were analyzed by inductively coupled plasma mass

spectrometry using a VG PlasmaQuad-3 at Duke University (Durham, North Carolina, USA). These data are presented and discussed in Kürkçüoğlu et al. (2015).

Clean chips of selected whole-rock samples, prepared with stainless steel tools, were separated for Sr-Nd-Pb-Hf isotopic analysis at San Diego State University (SDSU; San Diego, California, USA). Rock chips were cleaned first in ultrapure water (18 MW H_2O) followed by distilled 1N HBr, H_2O rinse, then distilled 2.5N HCl, and a final rinse in H_2O. They were then dissolved in a distilled HF-HNO_3 solution in sealed radius-bottom beakers perfluoroalkoxy (PFA) Teflon beakers on hot plates for a period of three days. Techniques for Pb, Sr, Hf, and Nd separation using anion exchange chromatography are described in Hanan et al. (2004, 2008). Sr isotopes were measured on a VG Sector 54 seven-collector thermal ionization mass spectrometer, and Hf, Nd, and Pb isotopes were analyzed on a Nu 1700 multi-collector inductively coupled plasma mass spectrometer following the methods of Hanan et al. (2004, 2008).

Measured $^{87}Sr/^{86}Sr$ isotope ratios were normalized to $^{88}Sr/^{86}Sr = 0.1194$ to correct for mass fractionation, and the Sr isotopic data are reported relative to the NIST SRM 987 standard ($^{87}Sr/^{86}Sr = 0.710250$). The Nd and Hf isotope ratios were corrected for instrumental mass fractionation and machine bias by application of a discrimination factor determined by bracketing sample runs with analyses of the SDSU AMES Nd and the JMC 475 standards, respectively (every two or three samples). Hf isotope sample data were normalized to $^{179}Hf/^{177}Hf = 0.7325$ and are reported relative to JMC 475 ($^{176}Hf/^{177}Hf = 0.282162$); Nd isotope sample data were normalized to $^{146}Nd/^{144}Nd = 0.7219$ and are reported relative to the lab value of $^{143}Nd/^{144}Nd = 0.512130$ for the SDSU AMES Nd standard. The measured value of $^{143}Nd/^{144}Nd$ of the La Jolla Nd standard at SDSU is 0.511844. Pb isotope ratios were monitored for isotope fractionation using the NIST SRM 997 Tl standard (White et al., 2000) and were corrected for instrumental mass fractionation and machine bias by applying a discrimination factor determined by bracketing sample analyses with analyses of NIST standard SRM 981 (every one or two samples) using values determined by Todt et al. (1996). The external reproducibility for $^{87}Sr/^{86}Sr$ and $^{143}Nd/^{144}Nd$ is 2 and 3 ppm, respectively; for $^{206}Pb/^{204}Pb$, $^{207}Pb/^{204}Pb$, and $^{208}Pb/^{204}Pb$ it is 21, 36, and 44 ppm, respectively; and for $^{176}Hf/^{177}Hf$ it is 2 ppm, based on replicate analyses of standards. Analytical results for procedural blanks were: <250 pg Sr, <200 pg Nd, <90 pg Pb, and <20 pg Hf. No blank corrections were applied to the data because they would have been insignificant.

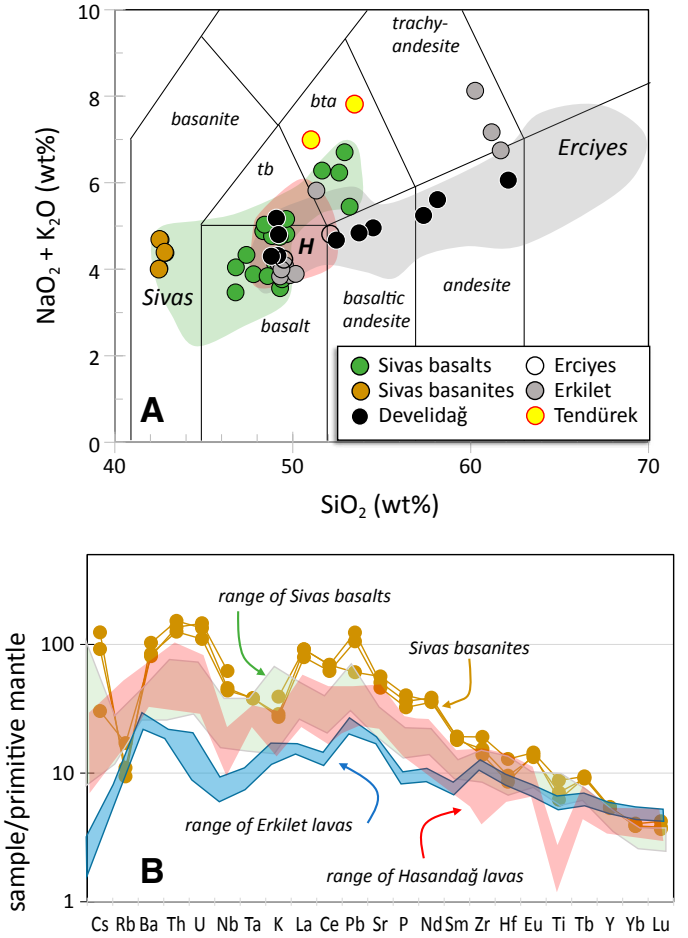

Figure 2. (A) Plot of total alkalis against silica for Central Anatolian lavas, showing individual samples discussed in this study and fields of published data. Red shaded field labeled "H" represents lavas from the Hasandağ cinder cone province. Field labels: bta—basaltic trachyandesite; tb—trachybasalt. (B) Primitive mantle–normalized trace element patterns of Sivas, Erkilet, and Hasandağ basalt suites (shaded) and Sivas basanites (normalizing values of Sun and McDonough, 1989). Sources of data: Aldanmaz et al. (2000, 2006, 2015); Kürkçüoğlu et al. (2001); Parlak et al. (2001); Alıcı et al. (2002); Chakrabarti et al. (2012); Reid et al. (2017); Gall et al. (2021); DiGiuseppe et al. (2018); Kocaarslan and Ersoy (2018).

RESULTS

Geochemistry of Central Anatolian Mafic Lavas

Young Sivas lavas comprising basalts through basaltic trachyandesites and subordinate basanites (Fig. 2) have been analyzed previously for their major and trace element compositions (Parlak et al., 2001; Kürkçüoğlu et al., 2015); five new analyses are included in Table 1. Incompatible trace element abundances of Sivas basanites show elevated Ba, Th, and U relative to the

TABLE 1. MAJOR AND TRACE ELEMENT GEOCHEMISTRY OF CENTRAL ANATOLIAN LAVAS

Location	Sivas	Sivas	Sivas	Sivas	Sivas	Erkilet	Erkilet	Erkilet	Erkilet	Erkilet	Erkilet	Erkilet	Erkilet	Erkilet	Erkilet	Erkilet
Age	Pliocene	Plio-Quaternary	Plio-Quaternary	Plio-Quaternary	Plio-Quaternary	Mio-Pliocene	Mio-Pliocene	Mio-Pliocene	Mio-Pliocene	Mio-Pliocene	Mio-Pliocene	Mio-Pliocene	Mio-Pliocene	Mio-Pliocene	Mio-Pliocene	Mio-Pliocene
Sample	OR2005-2	OR2005-1	TA2005-1	KA-2005-1	KA-2005-3	KY-07-6	KY-07-7	KY-07-2	KY-07-4	KY-07-5	KY-07-16	KY-07-9	KY-07-11	KY-07-12	KY-07-13	KY-07-1
UTM (N)	265283	265560	301891	344029	317443	710750	709624	708860	713171	713673	708168	708631	717500	709020	701879	705903
UTM (E)	4362149	4366197	4339380	4341404	4340560	4310760	4308737	4305309	4310039	4308815	4302875	4306906	4307106	4303597	4303697	4304082
Rock type	Basanite	Basalt	Basalt	Basalt	Trachybasalt	Basalt	Basalt	Basalt	Basalt	Basalt	Basalt	Basalt	Basaltic trachyandesite	Trachyte	Trachyte	Trachyte
Major elements (wt%)																
SiO_2	42.76	49.44	46.97	48.58	47.56	49.99	49.44	49.39	49.32	49.71	50.31	49.52	51.47	61.78	61.27	60.34
TiO_2	1.92	1.45	1.49	2.07	1.65	1.29	1.23	1.33	1.36	1.32	1.45	1.28	1.38	0.72	0.74	0.76
Al_2O_3	12.95	14.47	13.65	15.22	13.81	17.66	17.69	17.69	17.75	17.82	17.62	18.10	18.15	17.13	17.96	18.11
Fe_2O_3*	11.97	11.82	11.46	11.58	12.03	10.12	10.07	10.25	10.23	10.14	11.10	10.12	9.10	4.94	5.37	5.89
MnO	0.18	0.16	0.15	0.16	0.17	0.16	0.15	0.15	0.15	0.15	0.16	0.15	0.13	0.07	0.06	0.10
MgO	13.25	10.08	10.00	7.62	7.44	7.23	7.18	6.75	6.63	6.60	6.60	6.40	4.19	1.88	1.30	1.29
CaO	11.97	8.98	10.63	9.83	12.87	10.15	10.66	9.91	9.65	11.02	10.07	9.95	9.84	5.72	5.61	4.82
Na_2O	3.49	2.56	2.57	3.14	2.99	3.48	3.45	3.66	3.61	3.62	3.47	3.59	4.06	4.25	4.50	4.83
K_2O	1.17	0.98	1.45	1.87	1.32	0.36	0.37	0.46	0.52	0.45	0.40	0.39	1.74	2.48	2.65	3.28
P_2O_5	0.88	0.23	0.45	0.36	0.36	0.19	0.21	0.22	0.22	0.20	0.22	0.21	0.45	0.22	0.20	0.22
Total	100.54	100.17	98.82	100.43	100.20	100.63	100.45	99.81	99.45	101.03	101.41	99.70	100.51	99.18	99.68	99.65
LOI	n/a	n/a	n/a	n/a	n/a	0.32	1.28	0.26	0.62	1.02	0.72	0.61	1.29	1.64	1.37	1.39
Trace elements (ppm)																
Cs	0.97	0.12	0.26	0.12	0.16	0.05	0.06	0.06	0.08	0.08	0.10	0.07	0.41	1.06	2.42	1.32
Rb	10.8	12.8	15.5	17.4	13.2	4.55	4.61	5.35	5.13	4.58	4.18	4.35	25.1	57.6	75.1	81.0
Sr	1190	353	670	535	539	399	392	392	382	377	371	391	982	470	437	450
Ba	566	120	308	813	210	164	164	177	187	161	173	205	521	401	438	473
Sc	27.8	22.5	21.0	24.4	23.5	30.8	30.8	29.7	28.1	27.9	28.3	29.0	18.7	9.9	10.3	7.4
V	205.0	166.0	158.0	230.0	167.0	179.9	176.4	179.5	177.0	176.7	188.3	185.9	241.1	91.9	187.8	87.8
Cr	394	280	232	264	265	217	235	197	183	186	172	202	43	34	4	4
Co	65.6	53.8	42.7	94.4	43.9	59.2	65.6	64.0	92.2	57.2	62.2	60.5	52.1	32.7	43.7	26.8
Ni	332.0	195.0	229.0	89.8	210.0	113.9	131.5	111.9	108.8	98.1	79.6	110.8	36.5	18.4	5.4	1.6
Y	24.8	18.8	20.2	21.1	20.1	24.4	23.4	25.3	26.8	24.7	26.9	24.2	24.0	15.4	25.4	24.1
Zr	214	117	135	187	158	125	124	135	138	125	135	126	172	119	150	154
Nb	44.3	13.8	26.2	23.6	21.0	4.7	4.7	5.1	5.4	4.5	6.8	4.6	20.3	15.5	12.2	16.4
Hf	3.97	2.61	2.85	3.86	2.98	2.73	2.63	2.92	3.02	2.85	3.02	2.75	4.09	2.82	3.76	3.64
Ta	n/a	n/a	n/a	n/a	n/a	0.32	0.32	0.35	0.39	0.33	0.46	0.32	1.16	1.05	0.83	1.06
Pb	7.60	1.77	4.43	2.97	2.83	1.55	1.51	1.57	1.87	1.63	1.68	1.56	5.93	9.47	12.23	13.15
Th	11.57	2.20	5.20	2.56	3.69	1.62	1.64	1.70	1.79	1.64	1.82	1.61	6.92	8.26	10.86	11.20
U	3.07	0.66	1.04	0.62	1.10	0.26	0.38	0.42	0.40	0.19	0.25	0.25	1.55	2.67	3.46	2.99
Be	n/a	n/a	n/a	n/a	n/a	1.0	0.9	1.0	1.0	0.9	1.0	0.9	1.4	1.7	1.6	2.0
La	62.91	13.08	30.04	19.33	22.15	9.95	9.87	10.50	11.01	10.15	11.67	9.94	31.90	23.31	28.16	31.76
Ce	122.83	28.00	60.16	41.01	44.52	21.66	21.57	23.11	24.48	22.21	25.37	21.93	62.94	38.41	47.90	54.28
Pr	14.50	3.67	7.39	5.35	5.58	2.89	2.85	3.07	3.31	3.01	3.41	3.00	8.13	4.70	6.21	6.30
Nd	48.95	14.54	26.21	21.01	20.51	12.55	12.12	13.07	14.20	12.91	14.58	12.77	30.25	16.31	22.11	22.00
Sm	8.54	3.58	5.30	4.94	4.65	3.30	3.21	3.44	3.68	3.35	3.76	3.33	5.62	3.09	4.43	4.28
Eu	2.43	1.20	1.64	1.80	1.53	1.21	1.19	1.24	1.29	1.18	1.32	1.24	1.67	0.96	1.25	1.17
Gd	7.01	3.80	5.04	0.78	0.72	0.65	0.64	0.68	0.72	0.67	0.74	0.66	0.74	0.45	0.72	0.63
Tb	1.02	0.64	0.76	4.83	4.63	3.81	3.65	3.93	4.19	3.94	4.25	3.83	4.85	2.89	4.40	3.96
Dy	4.88	3.64	4.02	4.27	4.01	4.21	4.04	4.39	4.52	4.44	4.59	4.26	4.22	2.61	4.26	3.79
Ho	0.92	0.68	0.74	0.78	0.74	0.88	0.85	0.94	1.00	0.94	0.99	0.92	0.85	0.51	0.88	0.81
Er	2.25	1.66	1.81	1.91	1.79	2.50	2.33	2.59	2.77	2.57	2.72	2.52	2.36	1.40	2.49	2.33
Yb	1.91	1.53	1.55	1.65	1.54	2.43	2.27	2.47	2.67	2.49	2.60	2.38	2.18	1.39	2.45	2.34
Lu	0.27	0.22	0.22	0.23	0.22	0.35	0.33	0.36	0.39	0.36	0.38	0.35	0.32	0.22	0.34	0.34

Note: UTM indicates the Universal Transverse Mercator map projection system; data in this table are from zone 36S. Fe_2O_3* indicates that all iron was measured as trivalent. LOI indicates loss on ignition; samples were heated overnight at 110°C to drive off water and weights were taken prior and subsequent to heating. Samples for which no LOI measurements were made are indicated by n/a. n/a indicates that this element or parameter was not measured in the given sample.

basalts, corresponding negative Nb, Ta, and K anomalies, steeper rare earth element (REE) profiles (La/Sm_n ~4, where n refers to the chondrite-normalized abundance [normalizing values of Sun and McDonough, 1989]), and enrichment in REEs over high-field-strength elements of similar compatibility (Fig. 2).

Table 1 presents 11 new analyses of late Miocene–Pliocene basalts through basaltic trachyandesites from Erkilet volcano in north-central Anatolia (Fig. 1). The Erkilet lavas include seven geochemically homogeneous basalts with ~7 wt% MgO; their CaO/Al_2O_3 (~0.6) values overlap those of Sivas basalts with similar MgO, suggesting a similar crystallizing assemblage. Erkilet basalts have lower incompatible trace element abundances than Sivas basalts and show much less geochemical variability overall. Their primitive mantle–normalized incompatible trace element patterns have positive Ba anomalies and marked negative Nb-Ta anomalies.

Radiogenic Sr, Nd, Pb, and Hf Isotopes

From Central Anatolia, we analyzed the Sr-Nd-Pb-Hf isotopic compositions of 11 Sivas lavas including basanite, basalt, trachybasalt, and basaltic trachyandesite (Kürkçüoğlu et al., 2015). The new isotopic data presented in Table 2 also include 11 Miocene and younger lavas from Central Anatolia, specifically: five Erkilet lavas, four late Miocene–Pliocene Develidağ basalts, and two Quaternary Erciyes lavas; and new analyses of two basaltic andesites from Tendürek in Eastern Anatolia. The new Anatolian data have a wide range in isotopic values, with $^{206}Pb/^{204}Pb$ of 18.667–19.320, $^{207}Pb/^{204}Pb$ of 15.638–15.688, $^{208}Pb/^{204}Pb$ of 38.725–39.354, $^{87}Sr/^{86}Sr$ of 0.70366–0.70590, $^{143}Nd/^{144}Nd$ of 0.51257–0.51282, and $^{176}Hf/^{177}Hf$ of 0.28000–0.28302 (Table 2).

The data show a striking temporal variation in the binary ε_{Nd} versus ε_{Hf} plot (Fig. 3A) from Miocene through Quaternary time. Quaternary lavas from Central (Develidağ, Erciyes, Sivas, Hasandağ cinder cone province, Karapınar), Eastern (Tendürek), and Western Anatolia (Kula) and Central Anatolian late Miocene to Quaternary lavas from Erkilet define a broad field with intermediate ε_{Hf} (+4.11 to +9.50) and ε_{Nd} (−1.34 to +5.74) that extends above the terrestrial array to higher ε_{Hf} for a given ε_{Nd} relative to the Miocene data trend which falls about the terrestrial array (Fig. 3A; J. Blichert-Toft, personal commun., 2020). Two Sivas basanites plot along the terrestrial array, substantially closer to the field of northeastern Mediterranean sediments than the other Central Anatolian samples.

The $^{87}Sr/^{86}Sr$ versus ε_{Nd} plot (Fig. 3B) shows a temporal variation relationship analogous to that shown for ε_{Nd} versus ε_{Hf} (Fig. 3A). Our new samples collectively have Sr-Nd isotopic values that fall within the previously published range of Miocene and younger Central Anatolian mafic lavas (Wilson et al., 1997; Kürkçüoğlu et al., 2001; Parlak et al., 2001; Alici et al., 2002; Reid et al., 2017; DiGiuseppe et al., 2018; Gall et al., 2021). The Sr-Nd isotopic ranges for each volcanic area are restricted and define strong correlations (Fig. 3B). Sivas $^{87}Sr/^{86}Sr$ values range from 0.70399 to 0.70587 and $^{143}Nd/^{144}Nd$ from 0.51257 to 0.51280 (ε_{Nd} +3.12 to −1.34; Fig. 3); high-MgO basanites tend toward more-enriched Sr values. Develidağ and Erkilet basalts extend to slightly lower $^{87}Sr/^{86}Sr$ (0.7037) and higher ε_{Nd} (+3.61) values, while Erciyes basalts have ε_{Nd} between +0.5 and +1.6 and $^{87}Sr/^{86}Sr$ from ~0.704 to 0.705.

The Pb isotope signatures are consistent with those of the Sr, Nd, and Hf isotopes, showing temporal and spatial variations on Pb-Pb binary plots (Figs. 3C, 3D). In $^{206}Pb/^{204}Pb$ versus $^{207}Pb/^{204}Pb$ or $^{208}Pb/^{204}Pb$ space, the new data on late Miocene through Quaternary mafic lavas from Central Anatolia define a trend with a positive slope that is roughly parallel to the Northern Hemisphere reference line (NHRL) but at higher $^{207}Pb/^{204}Pb$ (15.597–15.657) and $^{208}Pb/^{204}Pb$ (38.503–39.334) for a given $^{206}Pb/^{204}Pb$ (18.667–19.320).

DISCUSSION

Petrogenesis of Sivas and Erkilet Mafic Lavas

Major element variations suggest that evolution of the Quaternary Sivas basaltic suite is controlled by as much as ~65% fractional crystallization of olivine (~16%), clinopyroxene (~35%), plagioclase feldspar (~40%), and Fe-Ti oxides (~9%) from a parental liquid with ~9 wt% MgO and ~47% wt% SiO_2 (Kürkçüoğlu et al., 2015). These lavas have primitive mantle–normalized incompatible trace element patterns with prominent negative anomalies for Nb, Ta, and K (Fig. 2) and steep REE profiles with La/Sm_n between 2.5 and 3.7. Pliocene Sivas basanites are not related to one another or to the basaltic lavas through crystal fractionation, i.e., P_2O_5 and K_2O contents of primitive basanites are elevated relative to those of the basalts and correlate positively with MgO (Kürkçüoğlu et al., 2015). Kürkçüoğlu et al. (2015) interpreted these samples as individual small-volume melts with significant contributions from a lithospheric source region metasomatically modified by fluids. Petrogenesis of the Erkilet lavas is not investigated here in detail. Their geochemical overlap with Sivas lavas suggests a comparable fractionating assemblage, while the shallow slope of their REE profiles (La/Sm_n ~2.0; Fig. 2) suggest they derive from melting within the spinel stability field.

Mildly alkalic mafic lavas from Central Anatolia were previously interpreted as asthenosphere-derived primary basaltic liquids that are heavily overprinted by crustal contamination (e.g., Parlak et al., 2001; Kocaarslan and Ersoy, 2018) or by interaction with mantle that has been modified by input of subduction-derived fluids (Notsu et al., 1995; Reid et al., 2017). Our data are not consistent with crustal contamination among parental mafic lavas, given that the Sr isotopic values of Central Anatolian lavas correlate poorly with MgO: Sivas lavas with >9 wt% MgO have the highest $^{87}Sr/^{86}Sr$ values (Fig. 4). This observation speaks against significant crustal contamination but rather supports an amended version of the latter model in which melts (and fluids?) of recycled continent-derived material located within the mantle dominate the isotopic and trace element signatures of the mafic lavas. Here we explore the mantle source domains and the temporal evolution of their contributions to Central Anatolian magmatism.

TABLE 2. Sr-Nd-Pb-Hf ISOTOPE COMPOSITIONS FOR CENTRAL AND EASTERN ANATOLIAN LAVAS

Region	Central	Central	Central	Central	Central	Central	Central	Central	Central	Central	Central	Central	Central	Central	Central	Central	Central	Central
Location	Sivas	Sivas	Sivas	Sivas	Sivas	Sivas	Sivas	Sivas	Sivas	Sivas	Sivas	Sivas	Develidağ	Develidağ	Develidağ	Develidağ	Develidağ	Develidağ
Age	Pliocene	Pliocene	Plio-Quaternary	Plio-Quaternary	Plio-Quaternary	Plio-Quaternary	Plio-Quaternary	Plio-Quaternary	Plio-Quaternary	Plio-Quaternary	Plio-Quaternary	Plio-Quaternary	Mio-Pliocene	Mio-Pliocene	Mio-Pliocene	Mio-Pliocene	Mio-Pliocene	Mio-Pliocene
Sample	OR2005-2	SV-16	SV-14	SV-08	OR2005-1	TA2005-1	SV-13	SV-10	SV-03	SV-01	SV-06	D2004-1	D2004-1 (p)	D2004-3	D2004-3 (p)	D2004-10 (p1)	D2004-10 (p2)	D2004-10	D2004-11 (p)
Rock type	Basanite	Basanite	Basalt	Basalt	Basalt	Basalt	Basalt	Basalt	Basalt	Trachybasalt	Basaltic trachyandesite	Basalt		Basalt		Basalt			Basalt
Notes		1	1	1			1	1	1	1	1	2	2	2	2	2	2	2	2
UTM (N)	265283	263385	257163	335596	265560	301891	312644	292582	336204	338301	303646	717074	717074	717256	717256	727255	727255	727255	726423
UTM (E)	4362149	4370578	4376133	3463249	4366197	4339380	4339398	4336204	4338851	4340133	4307511	4248686	4248686	4248456	4248456	4240021	4240021	4240021	4241120
$^{87}Sr/^{86}Sr$	0.705004	0.705865	0.705427	0.705045	0.704964	0.705016	0.704825	0.704385	0.704023	0.703987	0.704614	0.703656	0.703655	0.703698	0.703684	0.703942	n/a	0.703894	0.703902
$^{143}Nd/^{144}Nd$	0.512667	0.512570	0.512617	0.512655	0.512709	n/a	0.512692	0.512798	0.512777	0.512778	0.512691	n/a	0.512823	0.512818	n/a	0.512813	n/a	n/a	0.512807
ε_{Nd}	0.57	−1.34	−0.41	0.34	1.38	n/a	1.06	3.12	2.72	2.72	1.03	n/a	3.61	3.52	n/a	3.41	n/a	n/a	3.31
$^{206}Pb_i/^{204}Pb$	19.0338	19.0439	19.0270	18.9585	19.1080	18.9472	19.3195	19.0850	18.6669	18.6737	18.7316	18.9688	18.9650	18.9660	18.9692	18.9682	18.9726	18.9800	18.9488
$^{207}Pb/^{204}Pb$	15.6729	15.6827	15.6812	15.6683	15.6855	15.6666	15.6884	15.6576	15.6472	15.6378	15.6575	15.6527	15.6532	15.6527	15.6527	15.6561	15.6611	15.6539	15.6633
$^{208}Pb/^{204}Pb$	39.1227	39.1846	39.1318	39.0109	39.1197	39.0069	39.3542	39.0427	38.7393	38.7250	38.8366	38.9836	38.9816	38.9825	38.9832	38.9912	39.0067	38.9940	38.9890
$^{176}Hf/^{177}Hf$	0.283015	0.282966	0.282961	0.282938	0.282925	0.282955	0.282900	0.283001	0.282967	0.280000	0.282906	0.283007	0.283012	0.283016	0.283005	0.283009	n/a	0.283004	0.283010
ε_{Hf}	8.59	6.86	6.68	5.87	5.41	6.47	4.53	8.10	6.90	6.86	4.73	8.31	8.49	8.63	8.24	8.38	n/a	8.20	8.42

Region	Central	Central	Central	Central	Central	Central	Central	Eastern	Eastern
Location	Erciyes	Erciyes	Erkilet	Erkilet	Erkilet	Erkilet	Erkilet	Tendürek	Tendürek
Age	Quaternary	Quaternary	Mio-Pliocene	Mio-Pliocene	Mio-Pliocene	Mio-Pliocene	Mio-Pliocene	Quaternary	Quaternary
Sample	ERC95-64	ERC98-1	KY-07-6	KY-07-7	KY-07-2	KY-07-13	KY-07-1	28	31
Rock type	Basaltic andesite	Basalt	Basalt	Basalt	Basalt	Basaltic trachyandesite	Basaltic trachyandesite	Basaltic andesite	Basalt
Notes	3	3						4	4
UTM (N)	n/a	n/a	710750	709624	708860	701879	705903	n/a	n/a
UTM (E)			4310760	4308737	4305309	4303697	4304082		
$^{87}Sr/^{86}Sr$	0.704633	0.703832	0.704614	0.703742	0.703721	0.704695	0.704669	0.705895	0.705749
$^{143}Nd/^{144}Nd$	0.512720	0.512661	0.512806	0.512811	0.512814	0.512687	0.512689	0.512680	0.512680
ε_{Nd}	1.60	0.45	3.28	3.37	3.43	0.96	1.00	0.74	0.74
$^{206}Pb_i/^{204}Pb$	18.9085	18.9809	19.0956	19.0888	19.0832	18.9102	18.9072	18.8371	18.8306
$^{207}Pb/^{204}Pb$	15.6716	15.6535	15.6842	15.6766	15.6693	15.6706	15.6711	15.6556	15.6490
$^{208}Pb/^{204}Pb$	39.0073	38.9914	39.1671	39.1428	39.1173	38.9989	39.0126	38.8590	38.8443
$^{176}Hf/^{177}Hf$	0.282985	0.283006	0.283005	0.282996	0.282998	0.282998	0.282980	0.282888	0.282910
ε_{Hf}	7.53	8.28	8.24	7.92	7.98	7.99	7.36	4.10	4.88

Note: UTM indicates the Universal Transverse Mercator map projection system; data in this table are from zone 36S. (p) denotes analysis performed on powdered sample n/a indicates that this parameter was not measured in the given sample.
1. Major and trace element data in Kürkçüoğlu et al. (2015).
2. Major and trace element data in Kürkçüoğlu (2010).
3. Major, trace element, and Sr-Nd isotopic data from Kürkçüoğlu et al. (2001).
4. Major and trace element data in Şen et al. (2004).

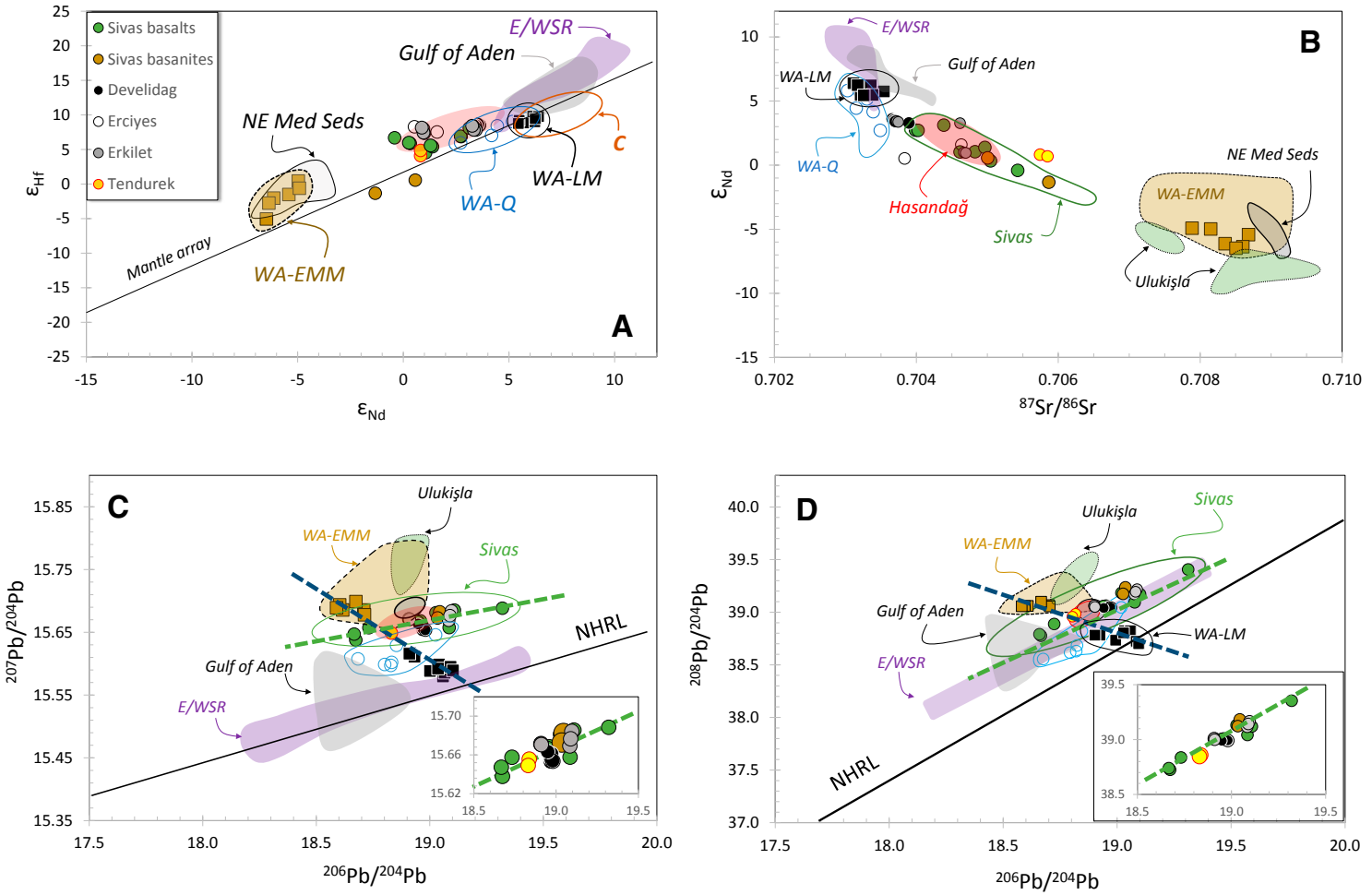

Figure 3. Sr-Nd-Pb-Hf isotopic variations in Anatolian lavas (Table 2; Aldanmaz et al., 2000, 2006; Alıcı et al., 1998, 2002; Chakrabarti et al., 2012; Reid et al., 2017; Gall et al., 2021). Data for early to mid-Miocene Western Anatolian lavas from Afyon, Simav, and Bigadiç (WA-EMM) and Quaternary Kula basalts (WA-Q) from Chakrabarti et al. (2012) are enclosed in the fields as drawn. Late Miocene Western Anatolia mafic lavas (WA-LM) plot within the range of the Gulf of Aden–Sheba Ridge (E/WSR) mid-ocean-ridge basalt (MORB) (Schilling et al., 1992; Rooney et al., 2011) and the global C component (Hanan and Graham, 1996). Also shown are fields for Hasandağ cinder cone province mafic lavas (red shading; Reid et al., 2017; Gall et al., 2021), Mediterranean Sea sediment samples taken near the Anatolian margin (NE Med seds; gray field with solid black line; Klaver et al., 2015), and the Late Cretaceous–Early Tertiary ultrapotassic Ulukişla lavas from Central Anatolia (green shading with dotted border; Alpaslan et al., 2004, 2006). (A) ε_{Hf}-ε_{Nd} values of Central Anatolian mafic lavas plot on and above the mantle array (J. Blichert-Toft, 2020, personal commun.). The Miocene and late Miocene through Quaternary data groups both trend toward the low-ε_{Hf} and low-ε_{Nd} field for modern northeastern Mediterranean Sea sediment. (B) Sr-Nd isotope ratios for late Miocene through Quaternary lavas from Central and Western Anatolia define near-linear arrays between the ambient MORB mantle with low $^{87}Sr/^{86}Sr$ and high ε_{Nd} and a heterogeneous Ulukişla and/or ocean sediment–like component. (C–D) $^{207}Pb/^{204}Pb$-$^{206}Pb/^{204}Pb$ (C) and $^{208}Pb/^{204}Pb$-$^{206}Pb/^{204}Pb$ (D) values of the younger Anatolian basalts plot above and roughly parallel to the range of Sheba Ridge MORB, whereas the tan field delineates the locus of the Miocene data. The composition of ambient sublithospheric MORB mantle is constrained by the intersection of the late Miocene data with the Gulf of Aden–Sheba Ridge and the Northern Hemisphere reference line (NHRL) MORB array. Inset panels show detail of Central Anatolian lavas.

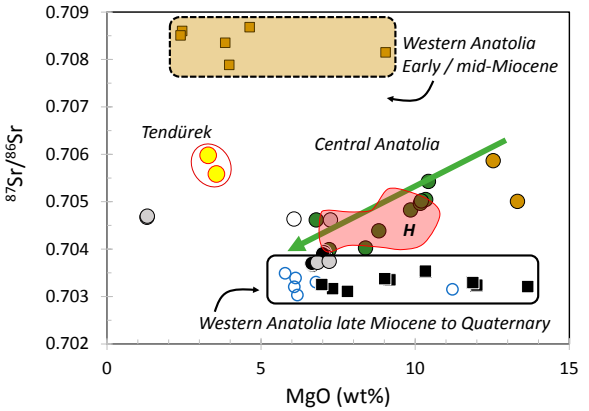

Figure 4. $^{87}Sr/^{86}Sr$ versus MgO for Anatolian lavas. Central Anatolia samples with >7 wt% MgO and Western Anatolia samples with >4 wt% MgO show no evidence for crustal contamination, which would result in a trend with slope opposite to that of the green arrow. More-evolved lavas from both regions have bulk geochemical relationships that are consistent with variable amounts of interaction between mantle lithospheric and sublithospheric materials. Symbols and sources of data are as in Figure 3.

Isotopic Characteristics of Anatolian Source Domains

The entire range of Central Anatolian Sr-Nd-Hf isotopic data falls within the broad array defined by Miocene and younger lavas from Western Anatolia, which encompasses widespread early and mid-Miocene lavas as well as late Miocene through Pliocene samples from Kula and Thrace (Aldanmaz et al., 2000, 2006, 2015; Alıcı et al., 2002; Chakrabarti et al., 2012). The ages of mafic volcanism in Western Anatolia are better constrained than those from Central Anatolia; samples reported here are categorized following whole-rock K-Ar determinations by Aldanmaz et al. (2000, and references therein). The early Miocene lavas have the highest $^{87}Sr/^{86}Sr$ (0.70835–0.70860) and the lowest ε_{Nd} (–6.24 to –5.89). Middle Miocene lavas range to less-radiogenic $^{87}Sr/^{86}Sr$ (0.70789–0.70868) and more-radiogenic ε_{Nd} (–5.19 to –4.68), while the late Miocene lavas cluster tightly at much-less-radiogenic $^{87}Sr/^{86}Sr$ (0.70311–0.70354) and more-radiogenic ε_{Nd} (+5.68 to +6.63). The late Miocene to Quaternary lavas from Kula (Aldanmaz et al., 2006; Chakrabarti et al., 2012) define a steeper trend with more variable $^{87}Sr/^{86}Sr$ values between 0.70303 and 0.70619 (Fig. 3B). In Western Anatolia, the early Miocene lavas of Foça and Yenişakran have lowest ε_{Hf} (–5.06 to –2.02) and ε_{Nd} (–6.24 to –5.89), increasing in the middle Miocene lavas of Foça, Ayvacık, and Bergama to ε_{Hf} of –1.52 to +0.46 and ε_{Nd} of –5.19 to –4.68), and jumping to very high ε_{Hf} (+8.84 to +9.85) and ε_{Nd} (+5.72 to +6.63) in the late Miocene lavas of Čanakkale, Thrace, Ayvacık, and Taştepe, similar to that of depleted mantle sources.

The Anatolian data set for Pb isotopic variations shows complex variations, given that the data do not define a single linear field or array in binary Pb-Pb space (Fig. 3). Specifically, late Miocene and younger lavas from Central Anatolia, Quaternary Western Anatolia mafic lavas, and Tendürek lavas in Eastern Anatolia define a trend in Pb-Pb isotopic space that is oblique to that of early Miocene through Pliocene Western Anatolian basalts. These Miocene lavas from Western Anatolia plot along negatively sloped trends that extend from the late Miocene data which plot near the NHRL ($^{206}Pb/^{204}Pb$ 18.910–19.102; $^{207}Pb/^{204}Pb$ 15.580–15.616; $^{208}Pb/^{204}Pb$ 38.649–38.753), through the middle Miocene data ($^{206}Pb/^{204}Pb$ 18.616–18.712; $^{207}Pb/^{204}Pb$ 15.686–15.678; $^{208}Pb/^{204}Pb$ 39.004–39.016), to the early Miocene data which plot at $^{207}Pb/^{204}Pb$ (15.689–15.693) and $^{208}Pb/^{204}Pb$ (39.005–39.048) and $^{206}Pb/^{204}Pb$ (18.589–18.675). We restrict our modeling and detailed interpretations to these high-precision data and published isotopic results for Western Anatolia lavas that have been comprehensively analyzed at San Diego State University using the procedures outlined herein (Aldanmaz et al., 2015).

The trends are seen most clearly in ternary Pb isotope space (Fig. 5) but are apparent in binary plots as well (Fig. 3). We recognize that the small number of samples from Eastern Anatolia makes a broad interpretation impossible but note that the high-precision data presented here are consistent with our geodynamic model for late Miocene through Quaternary lavas from across Anatolia. The positive Δ7/4Pb and Δ8/4Pb (i.e., the displacement of the samples from the NHRL; Hart, 1984), high $^{87}Sr/^{86}Sr$, and low ε_{Nd} observed for these lavas require a source component with older continent-derived Pb, Sr, and Nd isotope contents, i.e., higher values of Rb/Sr and lower Sm/Nd than the convecting mantle. In Sr-Nd isotope space, variations observed in Central Anatolia are analogous to those documented in the Gulf of Aden (the Sheba Ridge and its extension into the Gulf of Tadjoura; Fig. 3) where decreasing ε_{Nd} (from the Sheba Ridge to the Tadjoura Trough, Asal Rift, and Tadjoura Rift) reflects variable pollution of the upper mantle MORB source by recycled continent-derived material originating from the subcontinental lithospheric mantle (SCLM) and recycled oceanic lithosphere (Schilling et al., 1992; Rooney et al., 2011).

We interpret the Western Anatolian Miocene $^{206}Pb/^{204}Pb$-$^{207}Pb/^{204}Pb$ isotopic data array (Fig. 3) as a mixing trend and note that the intersection of the trend with the Gulf of Aden–Sheba Ridge MORB field and the NHRL characterizes the ambient upper-mantle isotope signature beneath Anatolia. This composition has distinctly more-radiogenic Pb isotopic values (and less-radiogenic Sr isotopic values) than the Quaternary Kula basalts that were interpreted by Chakrabarti et al. (2012) and Reid et al. (2017) to represent the depleted ambient end member. The Miocene trend can therefore be described as a mixture of two mantle sources, i.e., a grossly homogeneous ambient MORB source with $^{206}Pb/^{204}Pb$ of ~19, $^{207}Pb/^{204}Pb$ of ~15.6, and $^{208}Pb/^{204}Pb$ of ~38.6 and a heterogeneous lithospheric domain with lower $^{206}Pb/^{204}Pb$ but higher $^{207}Pb/^{204}Pb$ and $^{208}Pb/^{204}Pb$ that was modified by subduction-related contributions including direct melts of sediments and/or mélange.

Multi-component mixing is required to explain the isotopic signatures in late Miocene through Quaternary time as represented by lavas of these

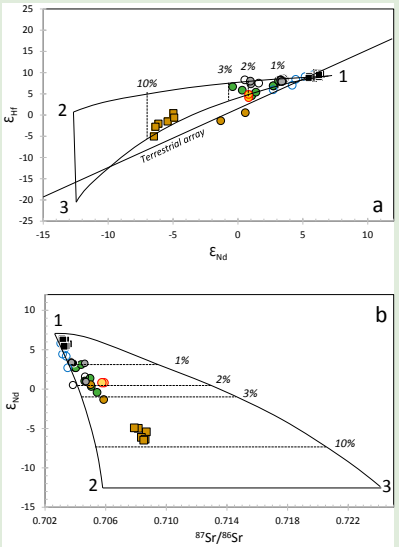

[1]Supplemental Material. Figure S1: The three end-member mixing model for the Anatolian lavas in (a) ε_{Nd}-ε_{Hf} and (b) ε_{Nd}-$^{87}Sr/^{86}Sr$ space. Table S1: Compositions of endmembers used in modeling. Please visit https://doi.org/10.1130/GEOS.S.15063120 to access the supplemental material, and contact editing@geosociety.org with any questions.

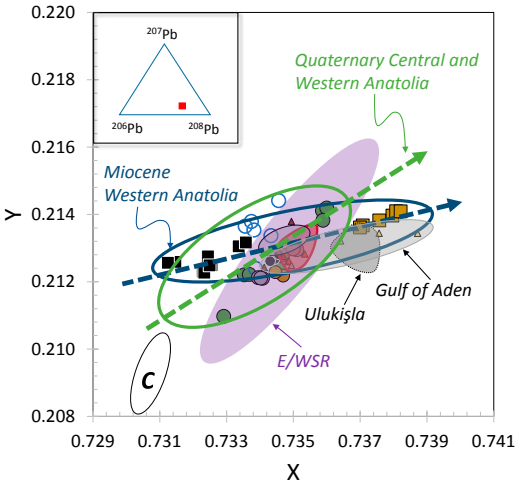

Figure 5. Relative ternary Pb isotope abundances in Anatolian mafic lavas show the difference in source components sampled by Miocene lavas from Western Anatolia (blue arrow) and late Miocene through Quaternary lavas from Central Anatolia (green arrow). The arrows represent linear regressions of the data in each group; the accompanying oval fields are schematic. The field of eastern Mediterranean sediments (dark gray border) lies at the intersection of the two trends and overlaps the field of samples from Hasandağ and Karapınar cinder cone provinces (red shading; Reid et al., 2017; Gall et al., 2021). A minimum of three end-member components is required to explain the distribution of the Pb isotope data: (1) a ^{206}Pb-rich component representing the ambient sublithospheric mid-ocean-ridge basalt (MORB) mantle source, and a heterogeneous subduction-modified component, similar to the source of the Ulukişla lavas and oceanic sediment, that varies in composition between (2) ^{207}Pb-rich and (3) ^{208}Pb-rich end members. Data sources and symbols are as in Figure 3. Axes are labeled in the ternary inset; the red square in the inset shows the location of the expanded slice in the ternary diagram. The plot shows relative proportions of ^{206}Pb, ^{207}Pb and ^{208}Pb (Rel ^{206}Pb, Rel ^{207}Pb, Rel ^{208}Pb), which can be plotted in x-y coordinates as X = Rel ^{207}Pb and Y = (Rel ^{208}Pb/sin (60°) + Rel ^{207}Pb/tan (60°)) (see Hanan et al., 1986, for theoretical and graphical details).

ages from Central and Eastern Anatolia and Quaternary basalts from Kula in Western Anatolia. Although the model parameters (Supplemental Table S1[1]) and results (Fig. 6; Fig. S1) are not unique, the end product is consistent with the available data and provides a geologically reasonable framework within which to interpret the genesis of the Anatolian suites. It takes at least three end-member components to bracket the compositional range of the Anatolian isotope data. We focus our discussion in Pb isotope space because variations of Pb isotopic values are very sensitive to mixing involving continent-derived recycled material. The identification of the sublithospheric ambient mantle as one end member requires a geometry where the remaining two end members have high Δ7/4Pb and Δ8/4Pb and plot in the Pb isotope region of continent-derived materials. The join between the two end members in Pb isotope space represents the range of heterogeneous source components (which vary in isotope composition and age) that have mixed with material derived from the ambient mantle to form the Anatolian lavas. One end member is characterized by radiogenic Pb isotopes with $^{206}Pb/^{204}Pb$ >19 similar to that of modern oceanic sediment, the other with $^{206}Pb/^{204}Pb$ ~18 similar to that of ancient sediment and/or continental lithospheric mantle.

We interpret the Western Anatolian late Miocene lavas with $^{206}Pb/^{204}Pb$ of ~19 to represent a sublithospheric component located in the upper mantle. For ease in modeling and visualization, we have chosen a single point located in the region of overlap between the Anatolian late Miocene data, Gulf of Aden–Sheba Ridge data, and NHRL to represent the ambient mantle isotope composition. Each of the Quaternary basalts represents a binary mix of a specific lithospheric composition along the join between the two continent-derived end members and this sublithospheric ambient mantle composition (see Table S1 [footnote 1]). The Anatolian lithosphere is envisioned as being isotopically heterogeneous, having undergone subduction-related enrichment resulting in pollution of the ancient lithosphere with younger recycled material, e.g., recycled sediment. Low-degree melts from subduction-modified lithosphere are known to be significantly enriched in Pb, Sr, Nd, and Hf (Hanan et al., 2008; Jean et al., 2014) relative to sublithospheric melts by factors of tens to hundreds. Multi-component mixing involving sediment with relatively high Pb (Sr, Nd, Hf) abundances can produce linear-like arrays in Pb isotope space, similar to the overall late Miocene–Quaternary array, that resemble binary mixing trends (Douglass and Schilling, 2000; Hanan et al., 2008). The isotope compositions of basalt derived by mixing between the MORB-like sublithosphere and Anatolian continental lithosphere components would be dominated by the continental lithosphere contribution because of its greater mass proportion of Pb, Sr, Nd, and Hf. This mixing scenario explains the origin of the Quaternary trend, with positive Δ7/4Pb and Δ8/4Pb subparallel to the MORB array, and the trends in $^{87}Sr/^{86}Sr$ and ε_{Hf} versus ε_{Nd} space extending between the sublithospheric ambient mantle (represented by the Western Anatolia early Miocene lavas) and oceanic sediment, including northeastern Mediterranean sediments and the Ulukişla ultrapotassic lavas derived from continental lithosphere. A similar argument can be made for the Miocene trend. For these samples, the heterogeneity in the continent-derived components is much less than in the Quaternary, so the trend of Miocene samples clusters about a single tie line between ambient mantle values and label 4 on the Pb isotopic model (Fig. 6).

The mixing model (Fig. 6) shows that the Miocene lavas have source contributions of continent-derived material ranging from <1% to <10%. The late Miocene to Quaternary Anatolian lavas, most of which are from Central Anatolia, can be modeled with contributions from lithospheric source domains of ~1%–3%. While the relationships are most pronounced in Pb-Pb plots,

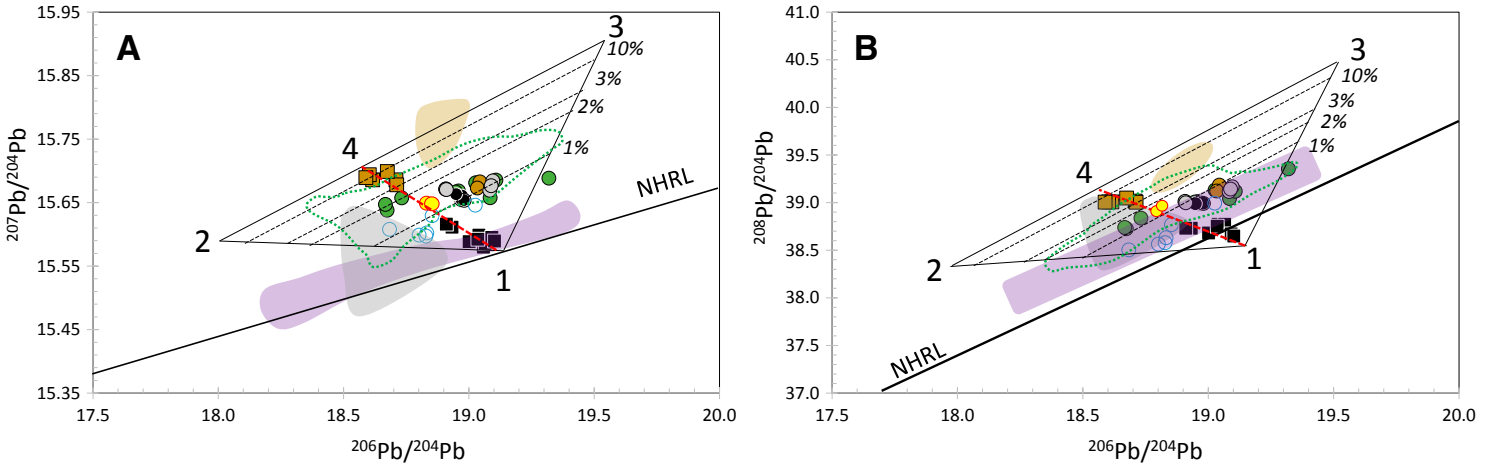

Figure 6. The three-end-member mixing model for the Anatolian lavas in $^{207}Pb/^{204}Pb$ (A) and $^{208}Pb/^{204}Pb$ (B) versus $^{206}Pb/^{204}Pb$ space. Reference fields are shown for oceanic sediments (dashed green line; White et al., 1986; Ben-Othman et al., 1989; Klaver et al., 2015) and the Ulukişla ultrapotassic lavas (brown field; Alpaslan et al., 2004, 2006). Fields for the Gulf of Aden (Schilling et al., 1992; Rooney et al., 2011) are shown in light purple for the Sheba Ridge and gray for the Asal Rift, Gulf of Tadjoura, and Tadjoura Trough. The Sheba Ridge field parallels the Northern Hemisphere reference line (NHRL; solid line) and is dominated by source mixing between the upper-mantle mid-ocean-ridge basalt (MORB) source and a young C-like recycled component (Hanan and Graham, 1996; Schilling et al., 1992; Rooney et al., 2011). The gray field for the Asal and Tadjoura data extends from that of the Sheba Ridge toward high Δ7/4Pb and Δ8/4Pb, indicative of the significant influence of ancient subcontinental lithospheric mantle (SCLM). The end-member isotope ratios and mass proportions are given in Table S1 (see text footnote 1). Source mixing in the Quaternary is modeled using end members 1 (ambient upper mantle), 2 (ancient continent-derived material), and 3 (relatively younger continent-derived source). The tie line 2-3 corresponds to the range of heterogeneity in the continent-derived source, and each point along it represents a distinct lithosphere and/or sediment Pb isotope composition. Each data point represents a unique mix that falls on a binary mixing line from 1 through the data point and intersecting the 2-3 tie line. The point of intersection represents the composition of the continent-derived source for that particular mix. The dashed lines labeled 10% to 1% represent the mass proportion of continent-derived material in the mixes where the mixing tie lines intersect. Note that the lithosphere and/or sediment end member for the Miocene (labeled 4) requires less of a range in $^{206}Pb/^{204}Pb$ and does not require as large a proportion of younger, radiogenic Pb. The Miocene data cluster closely about the line 1-4, showing that the heterogeneity in the continent-derived source was less pronounced at that time. Overall, the Miocene data have higher Δ7/4Pb and Δ8/4Pb than the Quaternary data, consistent with the influence of a SCLM source inferred for the Ulukişla ultrapotassic lavas and especially the Gulf of Aden, Asal Rift, and Tadjoura data. The parameter Δ7/4Pb is defined as: $100*[(^{207}Pb/^{204}Pb)_s–(^{207}Pb/^{204}Pb)_{NHRL}]$ and Δ8/4Pb is defined as: $100*[(^{208}Pb/^{204}Pb)_s–(^{208}Pb/^{204}Pb)_{NHRL}]$, where the subscript s indicates the value measured in the sample and the subscript NHRL refers to the Northern Hemisphere Reference Line of Hart (1984). Note that the Sr, Nd, and Hf isotope data are consistent with the Pb isotope mixing model results (Fig. S1) and are shown in the Supplemental Material (see text footnote 1) using the same symbols and labels.

ε_{Hf} versus ε_{Nd} and $^{87}Sr/^{86}Sr$ versus ε_{Nd} isotope plots are consistent with the Pb model (Fig. S1 [footnote 1]).

We note that the Miocene and Quaternary mixing trends defined in Pb isotope space by the Anatolian samples are similar to those observed in basalts from the Gulf of Aden, including the Sheba Ridge and its extension into the Gulf of Tadjoura (Schilling et al., 1992; Rooney et al., 2011), and suggest that these suites have similar source components. The Sheba Ridge data parallel the NHRL, and their isotope signature is dominated by mixing between the upper-mantle MORB source and a young C-like recycled mantle component (Schilling et al., 1992; Hanan and Graham, 1996; Rooney et al., 2011). The data field for the Sheba Ridge westward extension into the Gulf of Tadjoura (Asal Rift, Tadjoura Ridge, Gulf of Tadjoura) extends away from the Sheba Ridge in Pb isotope space toward high Δ7/4Pb and Δ8/4Pb, indicative of significant influence from ancient SCLM. The older Anatolian Miocene basalts are similar in isotope composition to the Asal Rift, Tadjoura Ridge, and Gulf of Tadjoura basalts due to the influence of older Pb presumably derived from the SCLM, whereas the Western Anatolian late Miocene and the Quaternary basalts resemble those of the Sheba Ridge in being more influenced by younger recycled Pb isotope signatures.

ROLE OF SEDIMENT CONTRIBUTIONS

Evidence from the Pb isotopes requires that mantle source regions of the Anatolian lavas have experienced pollution involving ancient crust and/or sediment and subduction products (e.g., fluids and/or melts). Specifically, early to mid-Miocene lavas from Western Anatolia all have Pb isotope compositions with high positive Δ7/4Pb and Δ8/4Pb that touch upon or overlap the field for

eastern Mediterranean sediments and Ulukişla ultrapotassic rocks (Figs. 3, 5). We note that sediments are enriched in Pb, Sr, Nd, and Hf over asthenospheric source components. The Late Cretaceous to middle Eocene Ulukişla suite is interpreted to be derived from a continental lithosphere mantle source that was metasomatized by fluids and/or melts generated during subduction (Alpaslan et al., 2004, 2006). We suggest here that the same geochemical characteristics could reflect incorporation of sediment and/or mélange into the sublithospheric source region (Behn et al., 2011; Nielsen and Marschall, 2017).

Support for this interpretation comes from the incompatible trace element abundances of early to mid-Miocene Western Anatolian lavas. When normalized to global oceanic sediment (GLOSS II; Plank, 2014), these samples exhibit essentially flat patterns anchored at unity, indicating the extent to which sediment contributions dominate the trace element signatures; the Ulukişla lavas show this same feature (Fig. 7). The trace element signatures of all other samples from Central Anatolia and the Quaternary Kula suite from Western Anatolia also have substantial overlap with GLOSS II but show differential enrichments and depletions that are likely inherited from sublithospheric sources. Specifically, both suites are depleted in large ion lithophile elements (including Pb) relative to GLOSS II, and the Kula lavas are enriched in Nb and Ta (Fig. 7). These features indicate the significance of sediment inputs and confirm the change in the source region(s) that we identified on the basis of Pb isotopic data (Fig. 5).

Contributions from sediments and subducted mélange material can be explored further through the abundances and isotopic signatures of Hf and Nd. These elements are effectively immobile in hydrous fluids (e.g., Kessel et al., 2005; Handley et al., 2011), and their similar compatibility in mantle phases means they are unlikely to fractionate during mantle melting or low degrees of crystallization in mafic melts. As a result, Hf-Nd fractionation is most likely to occur during melting of sediments or mélange (we use the term mélange following Nielsen and Marschall [2017] to indicate a physical

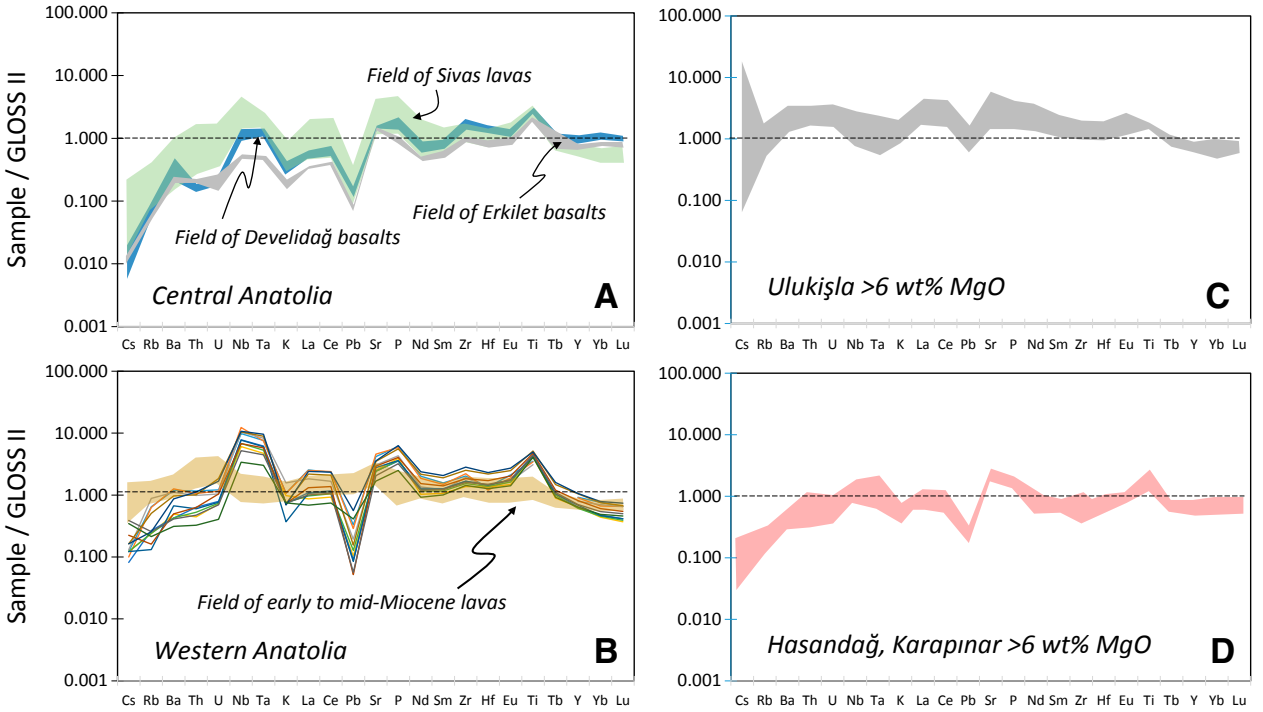

Figure 7. Incompatible trace element abundances in Anatolian lavas normalized to GLOSS II global oceanic sediment (Plank, 2014) show the importance of sediment contributions to the overall trace element budget of ultrapotassic Ulukişla lavas and early to mid-Miocene Western Anatolian basaltic lavas. Quaternary Western Anatolian mafic lavas from Kula (individual patterns shown) look very different from GLOSS II, suggesting insignificant sediment contributions. In Central Anatolia, two evolved Erkilet samples record substantial sediment contributions while mafic lavas from Develidağ, Hasandağ, Sivas, and much of Erkilet have patterns that require limited input from sediments and/or mélange.

mixture of sediments, altered oceanic crust, and hydrated mantle). Hf isotope values in oceanic sediment also vary independently from the Nd isotope values. This variation results from the "zircon effect" (Patchett et al., 1984), where sediments deposited close to their source have very low ε_{Hf} reflecting their detrital old zircon content; ocean sediments deposited further from the continent lack zircon and have relatively high ε_{Hf} controlled by the fine clay–rich continental material. Both Central and Western Anatolian lavas trend toward the high-ε_{Hf} field of oceanic sediment (Fig. 3). Note that the Central Anatolian late Miocene through Quaternary lavas trend to higher ε_{Hf} relative to contemporaneous Western Anatolian lavas, consistent with the idea that in the Central Anatolia region, where the Pb-Pb trends are subparallel to the MORB array, the mantle source for younger magmatism has experienced more subduction modification through incorporation of recycled oceanic sediments or sediment-derived fluids.

Variation in Nd isotopes as a function of Hf/Nd (Fig. 8) further delineates these mixing processes. Central Anatolian lavas define a broad mixing trend between mantle values and those of global and Mediterranean pelagic sediments (Nielsen and Marschall, 2017). This relationship indicates a role for direct contributions from sedimentary materials into the mantle source region. In detail, lavas from the Miocene and younger volcanic systems present a series of near-horizontal arrays of varying Hf/Nd at near-constant Nd isotopic compositions, interpreted as representing variable-degree melts of sediment

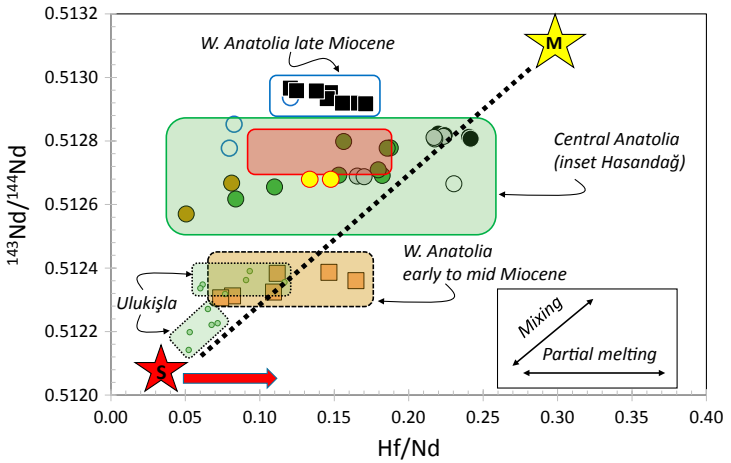

Figure 8. Trace element evidence for incorporation of sediment-derived materials in Anatolian lavas. Data sources are as in Figure 3. Schematic mixing model (following Nielsen and Marschall, 2017) shows that Ulukişla lavas can be considered isotopically as mixtures between melts of sediment (S) and ambient mantle (M). Variations in Hf/Nd at constant $^{143}Nd/^{144}Nd$ observed in several Anatolian mafic suites reflect melting of mélange subsequent to sediment-mantle mixing, rather than incorporation of slab-derived fluids in which Hf and Nd are immobile. This scenario suggests sediments and/or mélange are derived from delaminated slab(s) beneath Anatolia.

and/or mélange + mantle (i.e., mantle that has been contaminated by mixing prior to melting; Nielsen and Marschall, 2017). This relationship cannot reflect incorporation of slab-derived fluids in which both Hf and Nd are immobile. Compositions of Ulukişla ultrapotassic lavas approach those of pelagic sediments in this representation, consistent with their Sr-Nd-Pb isotopic systematics which suggest they represent infiltration of a sediment-derived melt into the lithosphere prior to magma formation. Western Anatolian lavas show consistent patterns that correspond to the age of magmatism. Early- to mid-Miocene lavas define distinct arrays that approach the Ulukişla and/or pelagic sediment values and extend to higher Hf/Nd reflecting variable degrees of mélange melting. Late Miocene lavas define a tight array, with compositions that lack significant contribution from sediment and/or mélange. Quaternary Kula basalts from Western Anatolia plot within and adjacent to the Central Anatolia array at intermediate values. These geographic and temporal relationships are consistent with the mixing inferred from Pb isotope relationships, in which a heterogeneous sublithospheric mantle interacts with much more heterogeneous contributions from a mixed lithospheric and/or mélange source domain with variable contributions from bulk sediments.

We emphasize that the proportion of sediments and/or mélange contributing to Anatolian magmatism is likely to be quite small (e.g., Klaver et al., 2015). Ancient continental lithosphere, rejuvenated by subduction processes, can contain high concentrations of Pb, Sr, Nd, and Hf relative to the ambient MORB sublithosphere mantle source (e.g., the Pb concentration in subduction-related fluids and metasomatized lithosphere can be tens to hundreds of times higher than in depleted mantle).

Implications for the Geodynamic Evolution of Anatolia

The picture that emerges from the geochemical signatures is one in which an abrupt change in source material occurs across all of Anatolia in the latest Miocene. Western Anatolia Miocene lavas were derived from a mixed source of subduction modified lithosphere and/or sediment and/or mélange and a MORB-like source region with $^{206}Pb/^{204}Pb$ >19. The $^{206}Pb/^{204}Pb$ of ~19 in the MORB-like late Miocene lavas suggests recent subduction enrichment in U, given that these samples plot near the NHRL. We interpret this to be due to the enhanced radiogenic growth of ^{206}Pb from ^{238}U decay relative to the decay ^{235}U, the parent of ^{207}Pb, which has a much shorter half-life. In contrast, latest Miocene through Quaternary lavas erupted in Western, Central, and Eastern Anatolia sample a distinct sublithospheric source that is relatively more isotopically heterogeneous due to subduction-process pollution by a young sediment component with radiogenic Pb isotopes like that of modern oceanic sediment. This is evidenced by the more-radiogenic $^{206}Pb/^{204}Pb$ and ε_{Nd}-ε_{Hf} values of the Central Anatolian trend relative to that of young Western Anatolian lavas. This shift marks a profound change in the mantle source regions for mafic volcanism.

The onset of slab rollback in the mid-Miocene appears to have been associated with an abrupt change in the isotopic characteristics of mafic lavas

(Seyitoğlu et al., 1997; Aldanmaz et al., 2000; Agostini et al., 2007; Chakrabarti et al., 2012; Ersoy and Palmer, 2013). Late Miocene Western Anatolian mafic lavas with high-precision Pb isotopic data (Figs. 3C, 3D) record the greatest contribution from the sublithosphere, presumably reflecting the flow of asthenospheric material following slab rollback, accompanied by rotation or tearing, in this region (Innocenti et al., 2005; Dilek and Altunkaynak, 2009; van Hinsbergen and Schmid, 2012; Ersoy and Palmer, 2013). Similarly, Agostini et al. (2008) found Li and B isotope variations in Biga Peninsula basalts that define an abrupt change from subduction-related to rift-related signatures prior to eruption of the Kula basalts, i.e., in the latest Miocene, a scenario that corresponds well to our interpretation of Sr-Nd-Pb-Hf isotopic data. The occurrence of 14–17 Ma post-collisional lamproites and ultrapotassic mafic lavas near the Kula eruptive area (Innocenti et al., 2005; Ersoy and Palmer, 2013) marks a turning point in the tectono-magmatic evolution of Western Anatolia, given that it was followed by mafic magmatism derived from source domains with increasing representation of less-metasomatized (i.e., sublithospheric) contributions. This scenario suggests that subduction of the Aegean or Tethyan seafloor took place throughout the region until the mid-Miocene (ca. 16–17 Ma), after which time rapid lithospheric thinning released subduction-related fluids that led to the eruption of these highly alkaline lavas (Agostini et al., 2008) and allowed for ascent of hotter sublithospheric material.

Isotopic and geochemical variations among Central Anatolian mafic lavas reflect spatially distinct melting scenarios of a shared heterogeneous mantle source in late Miocene through Quaternary time. Recent tomographic images suggest the presence of a delaminated Neotethyan slab beneath this region at a depth approaching that of the mantle transition zone, and mantle shear-wave splitting results suggest asthenosphere ascends beneath the Sivas area (Gans et al., 2009; Biryol et al., 2011; Bartol and Govers, 2014). The most recent phase of volcanism, e.g., in Sivas and Erkilet as described herein, occurred ~5 m.y. subsequent to delamination of the older slab and thus likely reflects melting of sediments and/or mélange along the top of the slab. We note that the greater depth of melting at Sivas (i.e., within the garnet stability field; Kürkçüoğlu et al., 2015) relative to more southern volcanic centers is consistent with this picture, given that the imaged depth to the top of the slab increases from south to north across Central Anatolia. We attribute the incorporation of bulk sediment and/or mélange (indicated by incompatible trace element abundances and Nd isotopic systematics; Fig. 8) as reflecting melting along the top of the descending, delaminated Tethyan slab in response to the ascent of warm asthenosphere (ambient mantle) through a tear in the subducted slab as imaged beneath Central Anatolia (Gans et al., 2009; Biryol et al., 2011). Farther south at Hasandağ, the Aegean slab displays multiple tears and fractures through and around which upwelling circum-Mediterranean asthenospheric mantle rises; heating along the base of the subcontinental lithosphere supports delamination melting at shallow levels (Reid et al., 2017; Gall et al., 2021) and may also affect sediments remaining along the delaminated slab itself at greater depth. Tectonic extension in the overlying plate likely also causes the asthenospheric material to rise to shallower depths and melt upon decompression.

CONCLUSIONS

New Sr-Nd-Pb-Hf isotopic results for mildly alkaline Anatolian mafic lavas reveal consistent spatial and temporal variations in mantle source mixing between lithospheric and sublithospheric source domains. The Pb isotopic signatures of Anatolian mafic lavas indicate a fundamental role for lithosphere that has interacted with mélange and/or sediments in the genesis of Pleistocene–recent volcanism. Despite the presumably volumetrically small contribution of sediment-derived melts and fluids, this material exerts a disproportionate control on the Pb (and Nd, Sr, and Hf) isotopic composition of the mafic silicate lavas. In Central Anatolia, latest Miocene through Quaternary lavas from Sivas, Develidağ, Erkilet, and Erciyes plot together with Quaternary lavas from Western and Eastern Anatolia in a region of Pb isotope space that is distinct from that of Miocene mafic lavas from Western Anatolia. The different isotopic groupings correspond to distinct mantle source regions, and this abrupt shift in contributing domains reflects a fundamental change in the geodynamics of the area.

We note that the isotope relationships and geochemical data support geophysical and tomographic models of the evolving upper-mantle structure beneath Anatolia. Delamination of the Neotethyan slab is inferred to have taken place in the early to mid-Miocene, and interaction between a sublithospheric component that represents the regional subduction modified ambient upper-mantle MORB source and slab-related materials such as sediments and mélange drives the isotopic composition of mafic lavas erupted across the region. One important implication of this result is that the subduction modification of mantle source regions contributing to Anatolian volcanism is not related solely to Miocene closure of Africa and Eurasia, but rather includes as well an older feature represented in sediments that melt along the top of the delaminated slab. Sampling of these domains occurs as upwelling sublithospheric subduction-modified MORB source material moves around and through the broken Aegean slab that dips steeply beneath southernmost Anatolia.

ACKNOWLEDGMENTS

This work was supported by grants from the U.S. National Science Foundation (EAR-0738963, DRL-0962792 to T.F.) and TUBİTAK (107Y215 to B.K.), and by the Pennsylvania State University Department of Geosciences Hiroshi and Koya Ohmoto Fellowship in Geosciences, Paul D. Krynine Memorial Fund, and Chevron Research Travel Award to M.P.S. B.B.H. gratefully acknowledges funding for the SDSU Mass Spectrometry Laboratory that has been provided by the MRI and OCE divisions of the U.S. National Science Foundation and the W.M. Keck Foundation. Comments from L. Farmer, A. Hofmann, J. Konter, and several anonymous reviewers helped to greatly clarify our thinking around the role of sediment in subduction zones.

REFERENCES CITED

Agostini, S., Doglioni, C., Innocenti, F., Manetti, P., Tonarini, S., and Savaşçin, M.Y., 2007, The transition from subduction-related to intraplate Neogene magmatism in the Western Anatolia and Aegean area, *in* Beccaluva, L., Bianchini, G., and Wilson, M., eds., Cenozoic Volcanism in the Mediterranean Area: Geological Society of America Special Paper 418, p. 1–15, https://doi.org/10.1130/2007.2418(01).

Agostini, S., Ryan, J.G., Tonarini, S., and Innocenti, F., 2008, Drying and dying of a subducted slab: Coupled Li and B isotope variations in Western Anatolia Cenozoic Volcanism: Earth and Planetary Science Letters, v. 272, p. 139–147, https://doi.org/10.1016/j.epsl.2008.04.032.

Aldanmaz, E., Pearce, J.A., Thirlwall, M.F., and Mitchell, J.G., 2000, Petrogenetic evolution of late Cenozoic, post-collision volcanism in western Anatolia, Turkey: Journal of Volcanology and Geothermal Research, v. 102, p. 67–95, https://doi.org/10.1016/S0377-0273(00)00182-7.

Aldanmaz, E., Köprübaşı, N., Gürer, Ö.F., Kaymakçı, N., and Gourgaud, A., 2006, Geochemical constraints on the Cenozoic, OIB-type alkaline volcanic rocks of NW Turkey: Implications for mantle sources and melting processes: Lithos, v. 86, p. 50–76, https://doi.org/10.1016/j.lithos.2005.04.003.

Aldanmaz, E., Pickard, M., Meisel, T., Altunkaynak, Ş., Sayıt, K., Şen, P., Hanan, B.B., and Furman, T., 2015, Source components and magmatic processes in the genesis of Miocene to Quaternary lavas in western Turkey: Constraints from HSE distribution and Hf-Pb-Os isotopes: Contributions to Mineralogy and Petrology, v. 170, 23, https://doi.org/10.1007/s00410-015-1176-x.

Alıcı, P., Temel, A., Gourgaud, A., Kieffer, G., and Gündoğdu, M.N., 1998, Petrology and geochemistry in the Gölcük area (Isparta, SW Turkey): Genesis of enriched alkaline magmas: Journal of Volcanology and Geothermal Research, v. 85, p. 423–446, https://doi.org/10.1016/S0377-0273(98)00065-1.

Alıcı, P., Temel, A., and Gourgaud, A., 2002, Pb-Nd-Sr isotope and trace element geochemistry of Quaternary extension-related volcanism: A case study of Kula region (western Anatolia, Turkey): Journal of Volcanology and Geothermal Research, v. 115, p. 487–510, https://doi.org/10.1016/S0377-0273(01)00328-6.

Alpaslan, M., Frei, R., Boztug, D., Kurt, M.A., and Temel, A., 2004, Geochemical and Pb-Sr-Nd isotopic constraints indicating an enriched-mantle source for Late Cretaceous to Early Tertiary volcanism, Central Anatolia, Turkey: International Geology Review, v. 46, p. 1022–1041, https://doi.org/10.2747/0020-6814.46.11.1022.

Alpaslan, M., Boztuğ, D., Frei, R., Temel, A., and Kurt, M.A., 2006, Geochemical and Pb-Sr-Nd isotopic composition of the ultrapotassic volcanic rocks from the extension-related Çamardı-Ulukışla basin, Niğde Province, Central Anatolia, Turkey: Journal of Asian Earth Sciences, v. 27, p. 613–627, https://doi.org/10.1016/j.jseaes.2005.07.002.

Aydar, E., Schmitt, A.K., Çubukçu, H.E., Akin, L., Ersoy, O., Sen, E., Duncan, R.A., and Atici, G., 2012, Correlation of ignimbrites in the central Anatolian volcanic province using zircon and plagioclase ages and zircon compositions: Journal of Volcanology and Geothermal Research, v. 213, p. 83–97, https://doi.org/10.1016/j.jvolgeores.2011.11.005.

Bartol, J., and Govers, R., 2014, A single cause for uplift of the Central and Eastern Anatolian plateau?: Tectonophysics, v. 637, p. 116–136, https://doi.org/10.1016/j.tecto.2014.10.002.

Behn, M.D., Keleman, O.B., Hirth, G., Hacker, B.R., and Massone, H.-J., 2011, Diapirs as the source of the sediment signature in arc lavas: Nature Geoscience, v. 4, p. 641–646, https://doi.org/10.1038/ngeo1214.

Ben Othman, D., White, W.M., and Patchett, J., 1989, The geochemistry of marine sediments, island arc magma genesis, and crust-mantle recycling: Earth and Planetary Science Letters, v. 94, p. 1–21, https://doi.org/10.1016/0012-821X(89)90079-4.

Biryol, C.B., Beck, S.L., Zandt, G., and Özacar, A.A., 2011, Segmented African lithosphere beneath the Anatolian region inferred from teleseismic P-wave tomography: Geophysical Journal International, v. 184, p. 1037–1057, https://doi.org/10.1111/j.1365-246X.2010.04910.x.

Chakrabarti, R., Basu, A.R., and Ghatak, A., 2012, Chemical geodynamics of Western Anatolia: International Geology Review, v. 54, p. 227–248, https://doi.org/10.1080/00206814.2010.543787.

Çoban, H., 2007, Basalt magma genesis and fractionation in collision- and extension-related province: A comparison between eastern, central and western Anatolia: Earth-Science Reviews, v. 80, p. 219–238, https://doi.org/10.1016/j.earscirev.2006.08.006.

Dewey, J.F., Helman, M.L., Turco, E., Hutton, D.H.W., and Knott, S.D., 1989, Kinematics of the western Mediterranean, *in* Coward, M.P., Dietrich, D., and Park, R.G., eds., Alpine Tectonics: Geological Society of London Special Publication 45, p. 265–283, https://doi.org/10.1144/GSL.SP.1989.045.01.15.

DiGiuseppe, P., Agostini, S., Manetti, P., Savaşçin, M.Y., and Conticelli, S., 2018. Sub-lithospheric origin of Na-alkaline and calc-alkaline magmas in a post-collisional tectonic regime: Sr-Nd-Pb isotopes in recent monogenetic volcanism of Cappadocia, Central Turkey: Lithos, v. 316–317, p. 304–322, https://doi.org/10.1016/j.lithos.2018.07.018.

Dilek, Y., and Altunkaynak, Ş., 2009, Geochemical and temporal evolution of Cenozoic magmatism in western Turkey: Mantle response to collision, slab break-off, and lithospheric tearing in an orogenic belt, *in* Van Hinsbergen, D.J.J., Edwards, M.A., and Govers, R., eds., Collision and Collapse at the Africa-Arabia-Eurasia Subduction Zone: Geological Society of London Special Publication 311, p. 213–233, https://doi.org/10.1144/SP311.8.

Dönmez, M., Türkecan, A., and Akçay, A.E., 2003, Kayseri-Niğde-Nevşehir yöresi Tersiyer volkanitleri: General Directorate of Mineral Research and Exploration of Turkey Report 10575.

Douglass, J., and Schilling, J.-G., 2000, Systematics of three-component, pseudo-binary mixing lines in 2D isotope ratio space representations and implications for mantle plume–ridge interactions: Chemical Geology, v. 163, p. 1–23, https://doi.org/10.1016/S0009-2541(99)00070-4.

Ersoy, E.Y., and Palmer, M.R., 2013, Eocene–Quaternary magmatic activity in the Aegean: Implications for mantle metasomatism and magma genesis in an evolving orogeny: Lithos, v. 180, p. 5–24, https://doi.org/10.1016/j.lithos.2013.06.007.

Gall, H., Furman, T., Hanan, B., Kürkcüoğlu, B., Sayit, K., Yürür, T., Sjoblom, M.P., Şen, E. and Şen, P., 2021, Post-delamination magmatism in south-central Anatolia: Lithos, v. 398, https://doi.org/10.1016/j.lithos.2021.106299.

Gans, C.R., Beck, S.L., Zandt, G., Biryol, C.B., and Ozacar, A.A., 2009, Detecting the limit of slab break-off in central Turkey: New high-resolution *Pn* tomography results: Geophysical Journal International, v. 179, p. 1566–1572, https://doi.org/10.1111/j.1365-246X.2009.04389.x.

Govers, R., and Fichtner, A., 2016, Signature of slab fragmentation beneath Anatolia from full-waveform tomography: Earth and Planetary Science Letters, v. 450, p. 10–19, https://doi.org/10.1016/j.epsl.2016.06.014.

Hanan, B.B., and Graham, D.W., 1996, Lead and helium isotope evidence from oceanic basalts for a common deep source of mantle plumes: Science, v. 272, p. 991–995, https://doi.org/10.1126/science.272.5264.991.

Hanan, B.B., Kingsley, R.H., and Schilling, J.-G., 1986, Migrating ridge-hotspot interactions: Pb isotope evidence in the South Atlantic: Nature, v. 322, p. 137–144, https://doi.org/10.1038/322137a0.

Hanan, B.B., Blichert-Toft, J., Pyle, D.G., and Christie, D.M., 2004, Contrasting origins of the upper mantle revealed by hafnium and lead isotopes from the Southeast Indian Ridge: Nature, v. 432, p. 91–94, https://doi.org/10.1038/nature03026.

Hanan, B.B., Shervais, J.W., and Vetter, S.K., 2008, Yellowstone plume–continental lithosphere interaction beneath the Snake River Plain: Geology, v. 36, p. 51–54, https://doi.org/10.1130/G23935A.1.

Handley, H.K., Turner, S., Macpherson, C.G., Gertisser, R., and Davidson, J.P., 2011, Hf-Nd isotope and trace element constraints on subduction inputs at island arcs: Limitations of Hf anomalies as sediment input indicators: Earth and Planetary Science Letters, v. 304, p. 212–223, https://doi.org/10.1016/j.epsl.2011.01.034.

Hart, S.R., 1984, A large-scale isotope anomaly in the Southern Hemisphere mantle: Nature, v. 309, p. 753–757, https://doi.org/10.1038/309753a0.

Innocenti, F., Mazzuoli, R., Pasquarè, G., Radicati Di Brozolo, F., and Villari, L., 1975, The Neogene calcalkaline volcanism of Central Anatolia: Geochronological data on Kayseri-Nigde area: Geological Magazine, v. 112, p. 349–360, https://doi.org/10.1017/S0016756800046744.

Innocenti, F., Agostini, S., Di Vincenzo, G., Doglioni, C., Manetti, P., Savaşçin, M.Y., and Tonarini, S., 2005, Neogene and Quaternary volcanism in Western Anatolia: Magma sources and geodynamic evolution: Marine Geology, v. 221, p. 397–421, https://doi.org/10.1016/j.margeo.2005.03.016.

Jean, M.M., Hanan, B.B., and Shervais, J.W., 2014, Yellowstone hotspot–continental lithosphere interaction: Earth and Planetary Science Letters, v. 389, p. 119–131, https://doi.org/10.1016/j.epsl.2013.12.012.

Keskin, M., 2003, Magma generation by slab steepening and breakoff beneath a subduction- accretion complex: An alternative model for collision-related volcanism in Eastern Anatolia, Turkey: Geophysical Research Letters, v. 30, 8046, https://doi.org/10.1029/2003GL018019.

Kessel, R., Schmidt, M.W., Ulmer, P., and Pettke, T., 2005, Trace element signature of subduction-zone fluids, melts and supercritical liquids at 120–180 km depth: Nature, v. 437, p. 724–727, https://doi.org/10.1038/nature03971.

Klaver, M., Djuly, T., de Graaf, S., Sakes, A., Wijbrans, J., Davies, G., and Vroon, P., 2015, Temporal and spatial variations in provenance of Eastern Mediterranean Sea sediments: Implications for Aegean and Aeolian arc volcanism: Geochimica et Cosmochimica Acta, v. 153, p. 149–168, https://doi.org/10.1016/j.gca.2015.01.007.

Kocaarslan, A., and Ersoy, E.Y., 2018, Petrologic evolution of Miocene-Pliocene mafic volcanism in the Kangal and Gürün basins (Sivas-Malatya), central east Anatolia: Evidence for Miocene anorogenic magmas contaminated by continental crust: Lithos, v. 310, p. 392–408, https://doi.org/10.1016/j.lithos.2018.04.021.

Kürkçüoğlu, B., 2010, Geochemistry and petrogenesis of basaltic rocks from the Develidağ volcanic complex, Central Anatolia, Turkey: Journal of Asian Earth Sciences, v. 37, p. 42–51, https://doi.org/10.1016/j.jseaes.2009.07.004.

Kürkçüoğlu, B., Sen, E., Aydar, E., Gourgaud, A., and Gündogdu, N., 1998, Geochemical approach to magmatic evolution of Mt. Erciyes stratovolcano Central Anatolia, Turkey: Journal of Volcanology and Geothermal Research, v. 85, p. 473–494, https://doi.org/10.1016/S0377-0273(98)00067-5.

Kürkçüoğlu, B., Sen, E., Temel, A., Aydar, E., and Gourgaud, A., 2001, Trace-element modelling and source constraints for tholeiitic and calc-alkaline basalts from a depleted asthenospheric mantle sources, Mt. Erciyes stratovolcano, Central Anatolia, Turkey: International Geology Review, v. 43, p. 508–522, https://doi.org/10.1080/00206810109465029.

Kürkçüoğlu, B., Pickard, M., Şen, P., Hanan, B.B., Sayit, K., Plummer, C., Sen, E., Yurur, T., and Furman, T., 2015, Geochemistry of mafic lavas from Sivas, Turkey and the evolution of Anatolian lithosphere: Lithos, v. 232, p. 229–241, https://doi.org/10.1016/j.lithos.2015.07.006.

Le Pennec, J.-L., Bourdier, J.-L., Froger, J.-L., Temel, A., Camus, G., and Gourgaud, A., 1994, Neogene ignimbrites of the Nevsehir plateau (central Turkey): Stratigraphy, distribution and source constraints: Journal of Volcanology and Geothermal Research, v. 63, p. 59–87, https://doi.org/10.1016/0377-0273(94)90018-3.

McClusky, S., Balassanian, S., Barka, A., Demir, C., Ergintav, S., Georgiev, I., Gurkan, O., Hamburger, M., Hurst, K., Kahle, H., and Kastens, K., 2000, Global Positioning System constraints on plate kinematics and dynamics in the eastern Mediterranean and Caucasus. Journal of Geophysical Research: Solid Earth, v. 105, p. 5695–5719, https://doi.org/10.1029/1999JB900351.

Meulenkamp, J.E., Wortel, M.J.R., Van Wamel, W.A., Spakman, W., and Starting, E.H., 1988, On the Hellenic subduction zone and the geodynamic evolution of Crete since the late Middle Miocene: Tectonophysics, v. 146, p. 203–215, https://doi.org/10.1016/0040-1951(88)90091-1.

Nielsen, S.G., and Marschall, H.R., 2017, Geochemical evidence for mélange melting in global arcs: Science Advances, v. 3, e1602402, https://doi.org/10.1126/sciadv.1602402.

Notsu, K., Fujitani, T., Ui, T., Matsuda, J., and Ercan, T., 1995, Geochemical features of collision-related volcanic rocks in central and eastern Turkey: Journal of Volcanology and Geothermal Research, v. 64, p. 171–191, https://doi.org/10.1016/0377-0273(94)00077-T.

Okay, A.I., and Tüysüz, O., 1999, Tethyan sutures of northern Turkey, *in* Durand, B., Jolivet, L., Horváth, F., and Séranne, M., eds., The Mediterranean Basins: Tertiary Extension within the Alpine Orogen: Geological Society of London Special Publication 156, p. 475–515, https://doi.org/10.1144/GSL.SP.1999.156.01.22.

Parlak, O., Delaloye, M., Demirkol, C., and Ünlügenç, U.C., 2001, Geochemistry of Pliocene/Pleistocene basalts along the Central Anatolian Fault Zone (CAFZ), Turkey: Geodinamica Acta, v. 14, p. 159–167, https://doi.org/10.1080/09853111.2001.11432441.

Patchett, P.J., White, W.M., Feldmann, H., Kielinczuk, S., and Hofmann, A.W., 1984, Hafnium/rare earth element fractionation in the sedimentary system and crustal recycling into the Earth's mantle: Earth and Planetary Science Letters, v. 69, p. 365–378, https://doi.org/10.1016/0012-821X(84)90195-X.

Plank, T., 2014, The chemical composition of subducting sediments, *in* Rudnick, R.L., ed., Treatise on Geochemistry (second edition), Volume 4: The Crust: Amsterdam, Elsevier Science, p. 607–629, https://doi.org//10.1016/B978-0-08-095975-7.00319-3.

Platzman, E.S., Tapirdamaz, C., and Sanver, M., 1998, Neogene anticlockwise rotation of central Anatolia (Turkey): Preliminary palaeomagnetic and geochronological results: Tectonophysics, v. 299, p. 175–189, https://doi.org/10.1016/S0040-1951(98)00204-2.

Reid, M.R., Schleiffarth, W.K., Cosca, M.A., Delph, J.R., Blichert-Toft, J., and Cooper, K.M., 2017, Shallow melting of MORB-like mantle under hot continental lithosphere, Central Anatolia: Geochemistry, Geophysics, Geosystems, v. 18, p. 1866–1888, https://doi.org/10.1002/2016GC006772.

Reilinger, R.E., McClusky, S.C., Oral, M.B., King, W., and Toksöz, M.N., 1997, Global Positioning System measurements of present-day crustal movements in the Arabian-Africa-Eurasia plate collision zone: Journal of Geophysical Research, v. 102, p. 9983–9999, https://doi.org/10.1029/96JB03736.

Rooney, T.O., Hanan, B.B., Graham, D.W., Furman, T., Blichert-Toft, J., and Schilling, J.-G., 2011, Upper mantle pollution during Afar plume–continental rift interaction: Journal of Petrology, v. 53, p. 365–389, https://doi.org/10.1093/petrology/egr065.

Schilling, J.-G., Kingsley, R.H., Hanan, B.B., and McCully, B.L., 1992, Nd-Sr-Pb isotopic variations along the Gulf of Aden: Evidence for Afar mantle plume–continental lithosphere interaction: Journal of Geophysical Research, v. 97, p. 10,927–10,966, https://doi.org/10.1029/92JB00415.

Şen, P.A., Temel, A., and Gourgaud, A., 2004, Petrogenetic modeling of Quaternary post-collisional volcanism: A case study of central and eastern Anatolia: Geological Magazine, v. 141, p. 81–98, https://doi.org/10.1017/S0016756803008550.

Şengör, A.M.C., and Yılmaz, Y., 1981, Tethyan evolution of Turkey: A plate tectonic approach: Tectonophysics, v. 75, p. 181–241.

Seyitoğlu, G., Anderson, D., Nowell, G., and Scott, B., 1997, The evolution from Miocene potassic to Quaternary sodic magmatism in western Turkey: Implications for enrichment processes in the lithospheric mantle: Journal of Volcanology and Geothermal Research, v. 76, p. 127–147, https://doi.org/10.1016/S0377-0273(96)00069-8.

Sun, S.-s., and McDonough, W.F., 1989, Chemical and isotopic systematics of oceanic basalts: Implications for mantle composition and processes, *in* Saunders, A.D., and Norry, M.J., eds., Magmatism in the Ocean Basins: Geological Society of London Special Publication 42, p. 313–345, https://doi.org/10.1144/GSL.SP.1989.042.01.19.

Temel, A., Gündoğdu, M.N., Gourgaud, A., and Le Pennec, J.-L., 1998, Ignimbrites of Cappadocia (Central Anatolia, Turkey): Petrology and geochemistry: Journal of Volcanology and Geothermal Research, v. 85, p. 447–471, https://doi.org/10.1016/S0377-0273(98)00066-3.

Todt, W., Cliff, R.A., Hanser, A., and Hofmann, A.W., 1996, Evaluation of a ^{202}Pb-^{205}Pb double spike for high-precision lead isotope analysis, *in* Basu, A., and Hart, S., eds., Earth Processes: Reading the Isotopic Code: American Geophysical Union Geophysical Monograph 95, p. 429–437, https://doi.org/10.1029/GM095p0429.

Türkecan, A., Acarlar, M., Dönmez, M., Hepşen, N., and Bilgin, R., 1998, Kayseri (Bünyan-Develi-Tomarza) yöresinin jeolojisi ve volkanik kayaçların petrolojisi: General Directorate of Mineral Research and Exploration of Turkey Report 10186: Ankara, 208 p.

Türkecan, A., Yıldırım, T., Satır, M., Harlavan, Y., and Açikgöz, S., 2000, Neogene volcanism of Sivas-Kangal-Gürün-Gemerek-Şarkişla area, *in* Özcan, Dora, O., Özgenç, İ., and Sözbilir, I., eds. International Earth Sciences Colloquium on the Aegean Region (IESCA) 2000 Abstracts: Izmir, Dokuz Eylül University, v. 114, p. 25–29.

van Hinsbergen, D.J.J., and Schmid, S.M., 2012, Map view restoration of Aegean–West Anatolian accretion and extension since the Eocene: Tectonics, v. 31, TC5005, https://doi.org/10.1029/2012TC003132.

White, W.M., Patchett, J., and BenOthman, D.B., 1986, Hf isotope ratios of marine sediments and Mn nodules: Evidence for a mantle source for seawater: Earth and Planetary Science Letters, v. 79, p. 46–54, https://doi.org/10.1016/0012-821X(86)90039-7.

White, W.M., Albarède, F., and Télouk, P., 2000, High-precision analysis of Pb isotope ratios by multi-collector ICP-MS: Chemical Geology, v. 167, p. 257–270, https://doi.org/10.1016/S0009-2541(99)00182-5.

Wilson, M., Tankut, A., and Guleç, N., 1997, Tertiary volcanism of the Galatia province, north-west Central Anatolia, Turkey: Lithos, v. 42, p. 105–121, https://doi.org/10.1016/S0024-4937(97)00039-X.

Wortel, M.J.R., and Spakman, W., 1992, Structure and dynamics of subducted lithosphere in the Mediterranean region: Verhandelingen van het Koninklijke Nederlands Akademie van Wetenschappen, v. 95, p. 325–347.

Yılmaz, Y., Yiğitbaş, E., and Genç, Ş.C., 1993, Ophiolitic and metamorphic assemblages of southeast Anatolia and their significance in the geological evolution of the orogenic belt: Tectonics, v. 12, p. 1280–1297, https://doi.org/10.1029/93TC00597.